A MINIATURE SIZE 3D PRINTED LINEAR PNEUMATIC ACTUATOR FOR ROBOTIC APPLICATIONS

by

CHRISTIAN L. TREVINO, B.S.

THESIS
Presented to the Graduate Faculty of
The University of Texas at San Antonio
in Partial Fulfillment
of the Requirements
for the Degree of

MASTER OF SCIENCE IN MECHANICAL ENGINEERING

COMMITTEE MEMBERS:
Pranav Bhounsule, Ph.D., Chair
Amir Jafari, Ph.D.
Amar Bhalla, Ph.D.

THE UNIVERSITY OF TEXAS AT SAN ANTONIO
College of Engineering
Department of Mechanical Engineering
December 2017

DEDICATION

I dedicate this work to my loving parents and sisters, whose support and encouragement throughout my years at UTSA helped me accomplish my goals both big and small. I also would like to thank and dedicate this work to my nephews and niece for their jokes, imagination, and smiles. I hope that one day they may be curious to also learn about engineering. Finally, I would like to dedicate this work to my loving fiancé, who has convinced me that I can do anything. I look forward to the great things he and I will engineer together, thank you.

ACKNOWLEDGEMENTS

I would like to thank my academic advisor, Dr. Pranav Bhounsule, for the great time and work that you have invested in each student's research and success in and outside of the Robotics and Motion (RAM) Laboratory at UTSA. As a member of the lab's team, I have grown as a researcher and student in the past few years and have seen those around me progress as well. I look forward to seeing the exciting future work that will come from the RAM lab. I would also like to thank my peer researchers, including Ali Zamani and Robert Brothers of the RAM lab for our many discussions of my research, which allowed me to greater understand my work. I would also like to thank the members, especially George Nall, of the Multifunctional Electronic Materials and Devices Research (MEMDRL) Laboratory at UTSA who helped me to fabricate a piezoelectric sensor for use with my linear pneumatic actuator. Finally, I would like to thank the rest of my thesis committee, including Dr. Amir Jafari and Dr. Amar Bhalla.

December 2017

A MINIATURE SIZE 3D PRINTED LINEAR PNEUMATIC ACTUATOR FOR ROBOTIC APPLICATIONS

Christian L. Trevino, M.S.
The University of Texas at San Antonio, 2017

Supervising Professor: Pranav Bhounsule, Ph.D.

3D printing has been used to create passive machines and mechanisms that require the integration of external actuators for movements. Printing actuators has the potential of expanding the utility of 3D printing, yet has little been explored. We have created a miniature size, double-acting, ON-OFF type, linear pneumatic actuator with a sufficiently high power to weight ratio using a hobby-grade Fused Deposition Modeling (FDM) 3D printer. The actuator has a bore size of 1.2 cm, a stroke length of 2.0 cm, and a wall thickness just under 0.2 cm. The overall weight of the actuator is 12 g and generates a peak output power of 2 W when operating at an input pressure of 40 psi. This thesis explores novel methods to solve the challenges that arise when during fabrication that include: (1) chemical processing to achieve airtight 3D printed parts with reduced surface roughness, (2) strategic placement of a metallic part for imparting strength, (3) O-ring design for a tight piston seal, and (4) chemical bonding of printed parts using adhesive. The power to weight ratio of our actuator is comparable to that of high-end commercial actuators of the same size. To demonstrate the utility of the actuator, we created a hopping Pixar lamp. Our conclusion is that 3D printed pneumatic actuators combine the high power of pneumatics with the low weight of plastics and structural strength through selective placement of metal parts, thus offering a promising actuator for robotic applications.

TABLE OF CONTENTS

Acknowledgements iv

Abstract v

List of Tables vii

List of Figures viii

Chapter One: Introduction to Actuators in Robotic Applications and their Common Design 1

How are Robots Actuated? 1

What are Pneumatic Actuators? 2

Common Designs of Current Linear Pneumatic Actuators 2

Pairing a Common Design paired with an Unlikely Fabrication Process 4

What is FDM 3D Printing? 4

Chapter Two: Hardware Design and Fabrication 6

Actuator Body 6

Chemical Post Processing 8

Part Bonding 15

Piston Head Design 16

Piston Rod 19

Piezoelectric Sensor Fabrication 23

Final Working Assembly 25

Summary of Failed Actuator Prototypes 25

Chapter Three: Experimental Setup 27

Experimental Setup 27

Determining Solenoid and Actuator Timing....28
Calibrating the Piezoelectric Sensor....29
Determining Actuator Operating Pressure....29
Chapter Four: Testing....31
Test: Actuators “Hopping” with Supports....31
Test: Outstroke Forces for Actuators on Rails....34
Test: Vertical Displacements for Actuators on Rails....37
Chapter Five: Comparison of A3 Actuator with Commercially Available Actuators....40
“Hobby Grade”, “Hobby Printed, and “High End” Actuators....40
Chapter Six: Actuator Implementation in a Robot....43
Pixar’s Luxo Jr. Lamp....43
Conclusion....46
References....48
Vita

LIST OF TABLES

Table 1 Mass Measurements for Various Testing Time Increments for a Cylindrical Sample with a Wall Thickness of 1.5 mm 11

Table 2 Calculated Values for Four O-Ring Designs for the Piston Head 18

Table 3 Timing Experiment to Determine the Timing for the Actuator 28

Table 4 Vertical Displacements for Actuators on Rails 37

Table 5 Results of Measured Vertical Displacement vs. Inlet Pressure 39

Table 6 Dimensions of Compared Actuators 42

Table 7 Performance Metrics of Compared Actuators 42

Table 8 A3 Actuator Dimensions 46

Table 9 A3 Actuator Performance Summary 47

LIST OF FIGURES

Figure 1 Images of Common Groups of Actuators in Robotic Applications 1

Figure 2 Early US Patent Images of Linear Actuators 3

Figure 3 Ultimaker 3 Extended 3D Printer along with a Component Breakdown 5

Figure 4 Computer Aided Designs (CADs) of a Double-Acting Linear Pneumatic Actuator Displaying Piston Head Areas for Both Outstroke and Instroke 6

Figure 5 Computer Aided Designs (CADs) of the Final Design, A3, Double-Acting Linear Pneumatic Actuator 7

Figure 6 Image of the Four Main 3D Printed Parts of the A3 Actuator Assembly 8

Figure 7 Images of the Actuator Head and End Cap with Cleaned Orifices 8

Figure 8 Graph of the Mass Measurements Versus Time for a Cylindrical Sample with a Wall Thickness of 1.5 mm 11

Figure 9 CAD STL Files from Cura of the Cylindrical Testing Vessels at Various Layer Depth…….. 12

Figure 10 3D Printed Cylindrical Vessels 13

Figure 11 Treated 3D Printed Cylindrical Vessels 13

Figure 12 Pressure Differential Results for Various Treated 3D Printed Cylindrical Vessels of Wall Thickness 1.5 mm 14

Figure 13 Surface Images of the Untreated and the 15 s Treated Testing Samples 15

Figure 14 Images of the Untreated and the 15 s Treated Parts 15

Figure 15 Images of the Bonding Adhesive as well as the Fully Assembled and Bonded Actuator…….. 16

Figure 16 Schematic of a Design for the O-Ring Gland of the Piston Head 17

Figure 17 Schematic of Compression Squeeze 17

Figure 18 Images of the Selected O-ring Design, Implemented with the Piston Head Fabricated Design 18

Figure 19 Image of Placement Process 20

Figure 20 Images of Horizontal Part Embedding 20

Figure 21 Images of Vertical Part Embedding and Piston Rod Assembly Design #1 21

Figure 22 Images of Piston Rod Assembly Design #2 21

Figure 23 Images of Piston Rod Assembly Design #3 and Post-Processing 22

Figure 24 Image of Piston Rod Assembly Design #4 23

Figure 25 Images of the Piezoelectric Crystal Measurements 23

Figure 26 Images of the Piezoelectric Crystal (Center) with Two Copper Electrode Sheets, Silver Epoxy, and Composite Sensor Structure 24

Figure 27 Piezoelectric Sensor Principle Figure and Circuit Schematic for the Piezoelectric Sensor…… .....

Figure 28 Image of the Final Fabricated Piezoelectric Sensor… 25

Figure 29 Views of the Final Assembly of A3 Actuator… 25

Figure 30 Image of Failed Actuator Prototypes… 26

Figure 31 Final Experimental Setup Hardware components used for Testing.....27

Figure 32 Timing Experiment to Determine the Timing for the Actuator. 28

Figure 33 Stress Induction within a Pressurized Cylinder. 29

Figure 34 Longitudinal Stress Failure of a Dynamically Tested Actuator. 30

Figure 35 Images of the A2 Actuator Hopper. 31
Figure 36 Images of the A2 Actuator Hopper during Successful Hop from Horizontal Plane.. 32
Figure 37 Images of the A2 Actuator Hopper during Failed Hop from Declined Plane……32
Figure 38 Images of the A3 Actuator Hopper 33
Figure 39 Images of the A3 Actuator Hopper during Successful Hop form Declined Plane.34
Figure 40 Images of the Experimental Setup for the Actuators on Rail 34
Figure 41 Images of the Fitted LEGO Actuator....35
Figure 42 Measured Output Force vs. Time (s) at Inlet Pressure 20 psi....35
Figure 43 Measured Output Force vs. Time (s) at Inlet Pressure 30 psi....36
Figure 44 Measured Output Force vs. Time (s) at Inlet Pressure 40 psi....36
Figure 45 Diagram of the Method of Vertical Displacement....37
Figure 46 Measured Vertical Displacement vs. Inlet Pressure for the A3 and LEGO Actuators…….....38
Figure 47 Comparing Various Commercial Actuators and the A3 Actuator....40
Figure 48 Scale of Various Compared Actuators 41
Figure 49 Image of Pixar's Luxo and Luxo Jr. 43
Figure 50 Image of CAD Assemblies in SolidWorks of Luxo Jr. Lamp Prototype....43
Figure 51 Image of Luxo Jr. 3D Printed Lamp Prototype 44
Figure 52 Images of Lamp Robot with Implemented A3 Actuator…….....44
Figure 53 Image of CAD Luxo Jr. Prototype in Matlab's Simscape 45
Figure 54 Final A3 Actuator compared in Size to a Lip Balm 46

CHAPTER ONE: INTRODUCTION TO ACTUATORS IN ROBOTIC APPLICATIONS

How Are Robots Actuated?

In robotics, there are many means of actuation. Actuation is what drives the movement of the robot at its joints. Common groups of actuators include: motors, hydraulics, pneumatics, shape memory allows, polymeric, piezoelectric, and magnetostrictive [5] .

Motors are commonly used in wheeled robots as seen in Figure 1 (a), while (b) is a quadrupedal, legged robot with hydraulic actuators. Many soft robots use low pressured pneumatics (Figure 1 (c)) where complex origami like geometries are inflated with air to grow in size and then are relieved, creating actuation. Flying bio-inspired robots, like that of Figure 1 (d) can have shape memory alloys that when paired with heat, can remember their original shape. Polymeric actuators are stimulated by an electric field, causing them to vary position (Figure X (e). Piezoelectric actuators (Figure X (f)) are high precision transducers with also convert electrical energy into motion. Lastly, Magnetostrictive actuators deform by strain when a magnetic field is present, a commercial device of such is seen in Figure X (g).

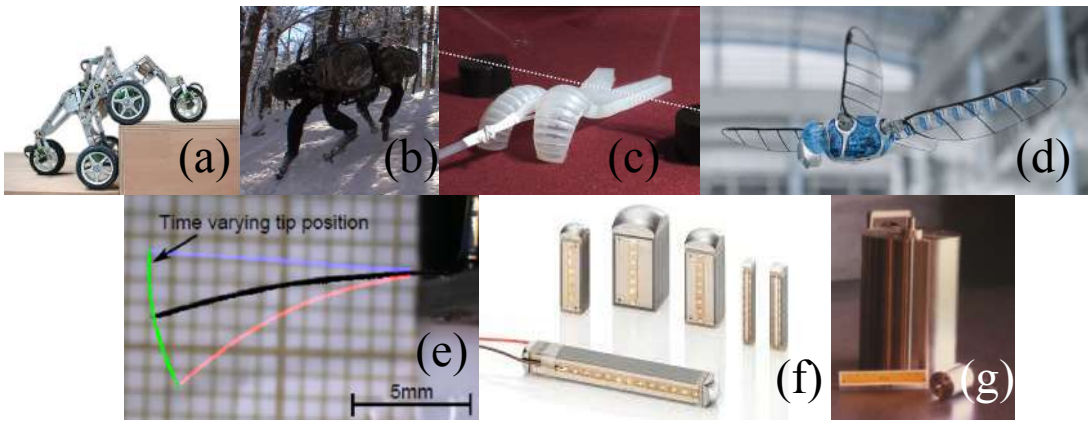

Figure 1: Images of Common Groups of Actuators in Robotic Applications

What Are Pneumatic Actuators?

Pneumatic actuation offers many advantages as a means of actuation. The compressed air that supplies the system is a clean, infinitely available fluid, easily moved and channeled, and can operate at a wide working temperature range. In robotics applications, pneumatic actuators are desirable due to their ability to produce high forces and achieve quick speeds. Little research has been done to date exploring the possibility of using Fused Deposition Modeling (FDM) 3D printers to fabricate small linear pneumatic actuators, which this thesis explores.

Common Designs of Current Linear Pneumatic Actuators

There are many published patents on fluid powered linear actuators, along with many variations in their design and control. Such publications include hydraulic and pneumatic powered actuators.

The US Patent 2,293,167 by J.W. Overbeke was a design of a hydraulically powered linear actuator dating back to August 18th, 1942 [Figure 2 (a)]. This patent focuses on a novel type of joint for securing the ends of the cylinder to lower leakage between part connections [1]. In March 6th, 1962, the US Patent 3,023,739 A [Figure 2 (b)] was published as “High Speed Pneumatic Actuator” by W.M., capable of reaching high speeds due to its novel double pneumatic cushion arrangement [2]. A published patent, US 3,202,062 by R.W. Burden displays his “Actuator” design [3], relating to a pivotal mount that allowed the design to be connected into a fluid powering system [Figure 2 (c)].

These three early patent designs of actuators, both hydraulic and pneumatic capable, focus on different aspects of fluid-powered linear actuator design including: fluid leakage between part connections of the overall assembly, fluid leakage between the piston head and the inner surface

of the cylinder, and external mount of an actuator for larger system implementation. Although these patents focus on only a few of the design considerations for linear, fluid powered actuators, they have a few things in common. The earliest designs for such actuators and more relevant designs share some basic common factors: (1) a main cylindrical body in which a (2) piston rod with a head capable of sealing fluid travels and is powered by a high pressure fluid that is readily available by (3) a number of inlet and outlet ports. These very basic design considerations were used a basis for the developed actuator design in this thesis.

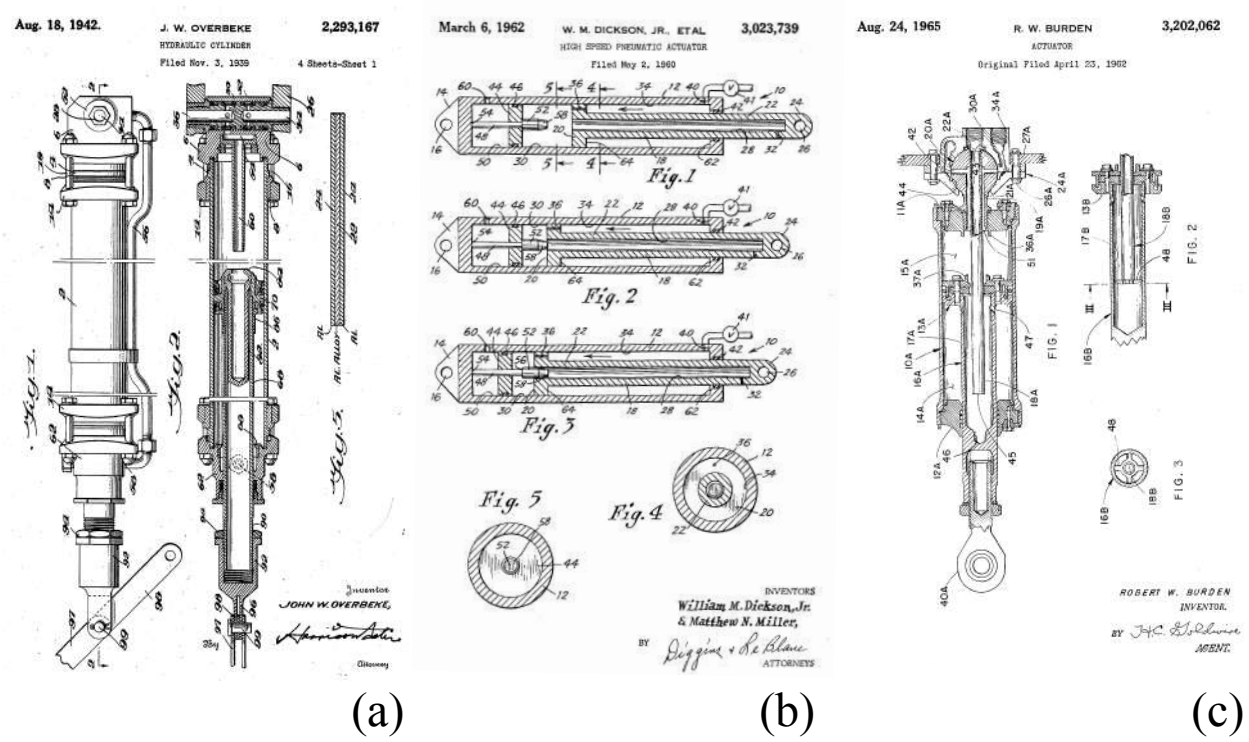

Figure 2: Early US Patent Images of Linear Actuators

When considering linear actuators, their style can be divided into two types, either single-acting or double-acting. “Single-Acting” refers to the actuator allowing the compressed air to act upon itself in a single direction, usually returned to its original position either with a spring or gravity. A “Double-Acting” cylinder allows for compressed air to act upon the piston head in two

directions opposite of each other [4]. Due to an increased number of robotic application possibilities, the later introduced actuator design was developed as double-acting, allowing for the control of both the extension and retraction of the piston rod. Further details of the multiple components that attribute such a design are expressed in detail in Chapter 2.

Pairing a Common Design with an Unlikely Fabrication Process

The mechanical design of the actuator presented in this thesis is not novel, as its components are based on many designs that have come before it. However, the fabrication process chosen to create the actuator proved to be experimental. The fabrication process chosen was one of today's most common and available means of 3D printing- Fused Deposition Modeling (FDM). The process was chosen due to its availability, low operating costs, and ease of use. Due to its commonality as a "hobby" printing process, the design may also be easily shared with other researchers and interested persons that may want to explore or contribute to furthering such research in 3D printed actuators.

What is FDM 3D Printing?

FDM 3D printing is an additive manufacturing process in which a thin cylindrical filament, in the case of this research has a diameter of 0.4 mm, is vertically fed through a heated nozzle and deposited onto previous layers. This assembly of layers sits upon itself and when cooled, binds with its previous deposits. Room for the vertical growth of such a composition is provided by a lowering and sometimes heated "bed" or "build plate". The FDM 3D printed used in this research was an Ultimaker 3 Extended printer [6]. An image of the used 3D printer as well as its component breakdown can be seen in Figure 3 (a) and (b). The printer advertises the capability of printing layers 200 to 20 microns in resolution with a nozzle of diameter size: 0.40 mm. It also

states an XYZ accuracy of 12.5, 12.5, and 2.5 microns. While the printer supports printing materials of: Nylon, Polylactic Acid (PLA), Acrylonitrile Butadiene Styrene (ABS), Co-Polyester (CPE), Co-Polyester (CPE+), PolyVinyl Alcohol (PVA), Polycarbonate (PC), Thermoplastic Polyurethane (TPU 95A), and Polypropylene (PP), an explanation as to why ABS was selected will be presented in Chapter 2.

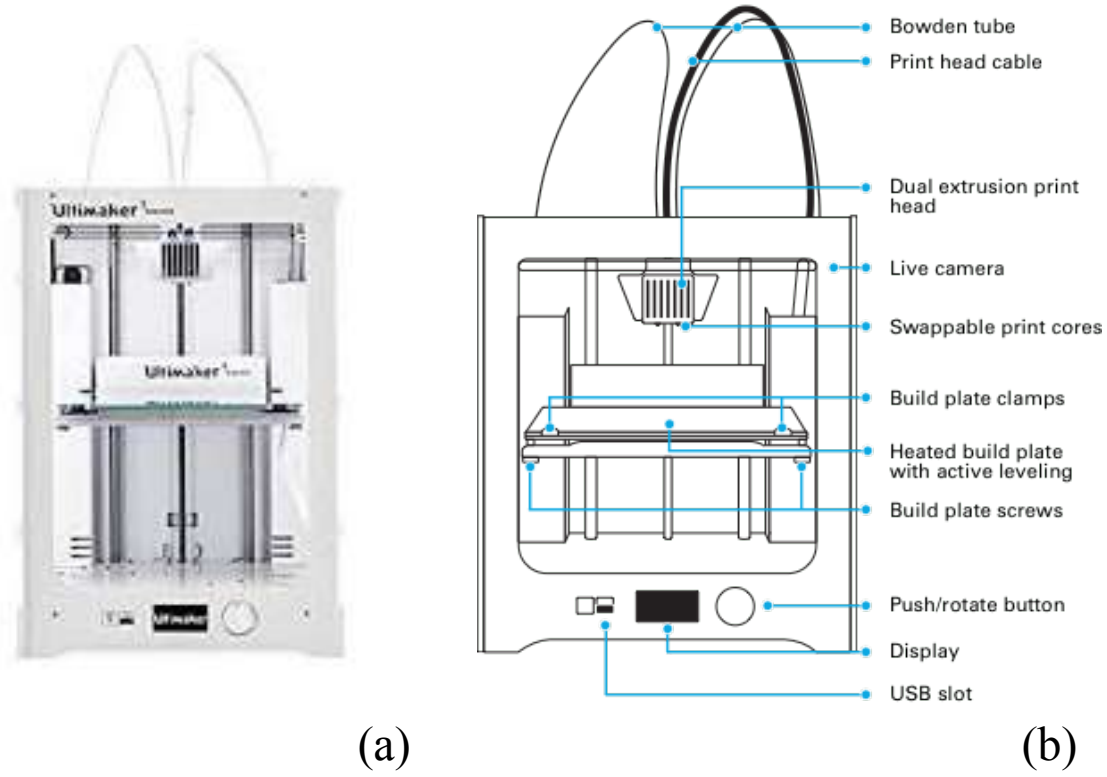

Figure 3: Ultimaker 3 Extended 3D Printer along with a Component Breakdown

CHAPTER TWO: HARDWARE DESIGN AND FABRICATION

Actuator Body

The general force equation,

$$F=pA \quad \text{(eq. 1)}$$

where the force is equal to the pressure times the area of the piston head is used to calculate the theoretical output force that a linear pneumatic actuator will generate. For calculating the force of the outstroke, the area is equal to $[\pi(d_1^2/4)]$ and when calculating the force of the instroke, the area is equal to $[\pi(d_1^2-d_2^2)]/4$. The outstroke force will be greater than the instroke force for designs similar to Figure 4, which is the designed A3 Actuator to be discussed throughout the paper.

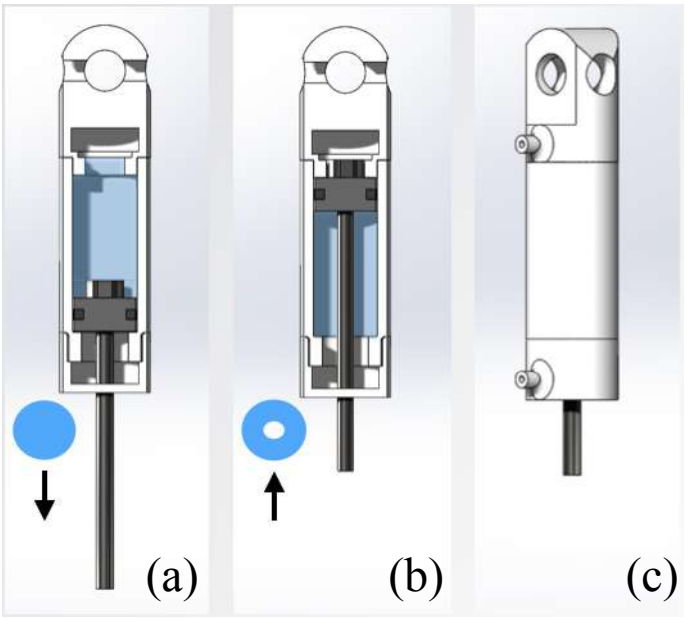

Figure 4: Computer aided designs (CADs) of a Double-Acting Linear Pneumatic Actuator Displaying Piston Head Areas for Both Outstroke and Instroke

Figure 4 (a) displays the cross-sectional view of a double-acting actuator in a fully extended linear position, applying an outstroke force. Figure 4 (b), also a cross-sectional view of

the actuator, displays the opposite- a fully retracted linear position of an applied instroke force. In both (a) and (b), blue schematics are shown which represent the applicable area that the compressed air act upon during the actuation processes.

As seen in Figure 4 (c), a double-acting linear pneumatic actuator consists of two ports. These two ports toggle back and forth (due to a solenoid valve) as being either inlet or outlet ports. These ports are both connected to a solenoid valve via tubing.

The final CAD design for the A3 actuator can be seen in Figure 5. The body of the actuator comprised of a 6 part assembly that included the (1) actuator head with port A, (2) cylinder, (3) piston head, (4) O-ring, (5) end cap with port B, and the (6) piston rod.

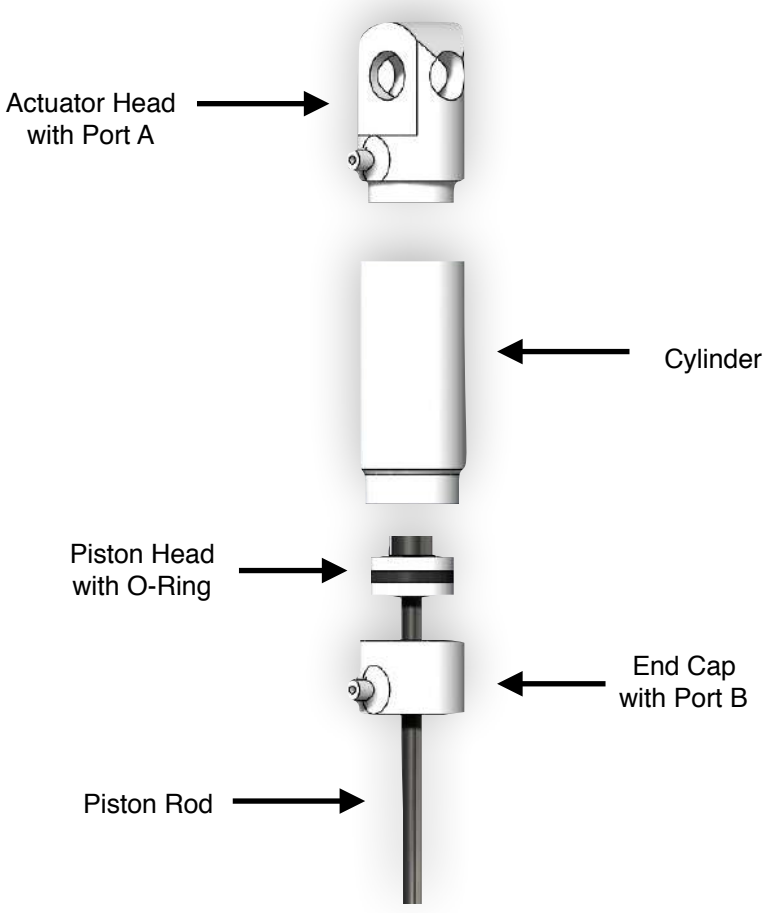

Figure 5: Computer Aided Designs (CADs) of the Final Design , A3, Double-Acting Linear Pneumatic Actuator

Chemical Post-Processing

The actuator assembly is comprised of 4 main 3D printed parts: the Piston Head, End Cap, Actuator Head, and the Cylinder. These parts can be seen in Figure 6 in their respective ideal printing orientations for the Fused Deposition Modeling (FDM) process 3D printer that was used for their fabrication. The parts are printed using Acrylonitrile Butadiene Styrene or more commonly known as “ABS”.

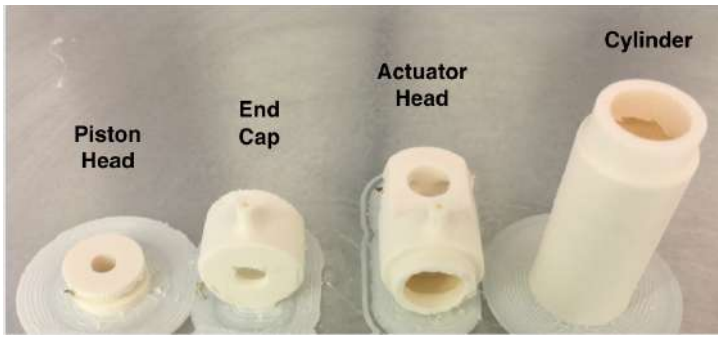

Figure 6: Image of the Four Main 3D Printed Parts of the A3 Actuator Assembly

Once the parts are completed printing, they are removed carefully from the build plate and excess material is either lightly cleaned with a fine grit sand paper, or cut away with an X-Acto blade. For the fairly small in diameter holes of the two ports, one in the actuator head and the second in the end cap, a thin, metallic needle is used to discharge any debris or excess ABS material. The process can be seen in Figure 7 (a) and (b).

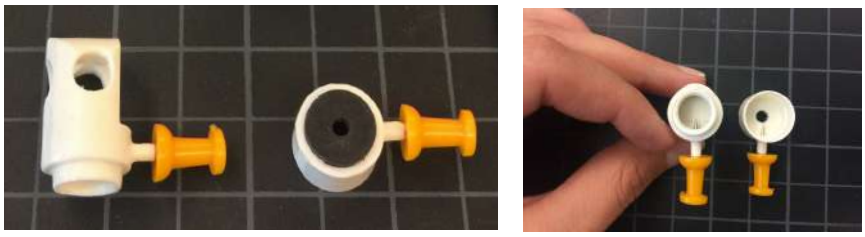

Figure 7: Images of the Actuator Head and End Cap with Cleaned Orifices

Once all of the 3D printed parts are cleaned of their excess material,they are washed and rinsed with soap and water and left to fully dry. Upon drying, the parts are then chemically treated with a 15 second dip in Acetone.

When the parts were fully dry from chemical treating, they were then bonded together to create the full actuator assembly. Bonding of the ABS parts was accomplished by using Ethyl Cyanoacrylate. Together, the two react to create a strong surface bond. There are other methods to bonding the parts, however, this particular adhesive method offers the following advantages (assuming proper application): distributes loads/stresses evenly, resists flex and vibrational assemblies, forms a seal as well as a bond, barely increases the overall mass of the assembly, virtually no change is applied to the part dimensions or the geometry of the parts, and is a quick and easy bond for heat-sensitive materials, such as the thermoplastic-ABS. There are however, a couple of disadvantages to bonding with Cyanoacrylate. One is that it does not bond well to smooth surfaces, for this reason, all of the surfaces for the parts that need to be bonded are left without sanding. Another challenge when working with both ABS, Acetone, and Cyanoacrylate is that Acetone actually acts as a solvent for Cyanoacrylate. Therefore, all of the chemical treating with Acetone of the parts is done and left to fully dry before being exposed to and bonded with Cyanoacrylate.

ABS plastic was chosen for printing due to its mechanical properties and chemical relationship with Acetone. ABS is a thermoplastic polymer, amorphous, that has a high impact resistance and toughness [9]. More importantly however, ABS and Acetone are a desirable pair for pneumatics applications for a couple important reasons. ABS can undergo surface treatments with Acetone that can create sealing of the material from escaping compressed air as well as

improve surface roughness for cyclic interaction between parts such as the inner surface of the cylinder and the piston head.

Acetone will dissolve ABS and when applied directly to ABS, allows for material displacement. Chemical energy is added from the Acetone to the polymer, in turn allowing it to displace before drying and hard setting. [10]

The duration of the chemical treatment for the parts, 15 seconds, was determined by a series of experimental tests. First, another method using Acetone vapor was conducted on a set of ABS parts. The parts were placed in a sealed container, positioned for optimal exposure of the vapors. The parts did not come into direct contact with the liquid fluid itself. The method proved significantly slower with effective timescales ranging from 1 hour to 10+ hours.

Based on the lengthy testing time of the previous method, another method was explored. A new set of printed ABS parts were tested for different durations submerged in liquid acetone. The samples tested had similar dimensions to those of the cylinder used in the actuator assembly including the same radii, wall thickness, yet were 1/2 the overall length of the actuator cylinder. A single ABS sample was tested to determine the rate at which it dissolved in a container of liquid Acetone. The sample was weighed incrementally to determine loss of ABS mass transferred from the sample to the liquid Acetone. The numerical results can be seen in Table 1, as well as in corresponding graphical form in Figure 8.

Table 1: Mass Measurements for Various Testing Time Increments for a Cylindrical Sample with a Wall Thickness of 1.5 mm

	Mass Measurement (g), (oz)
t=0s	2, 0.07
t=20 mins	1.42, 0.05
t=40 mins	1, (part failure)
t=60 mins	0.5, 0.02
t=80 mins	0.4, 0.02
t=100 mins	0.4, 0.02

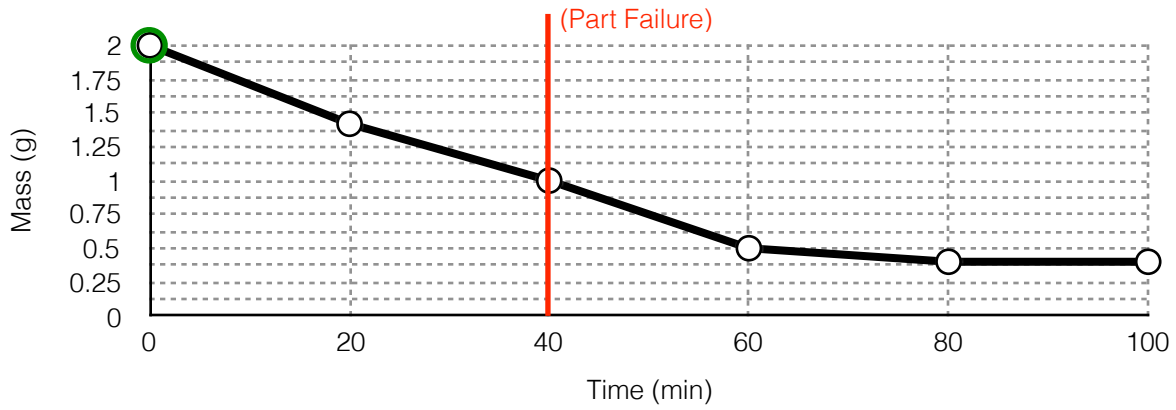

Figure 8: Graph of the Mass Measurements Versus Time for a Cylindrical Sample with a Wall Thickness of 1.5 mm

The cylindrical samples can be seen in the figure X. The first two images display two adjacent printed layers, clearing displaying the perpendicular layering of the slicing design. The third image displays the slicing design for the cylindrical wall. The outer diameter of the cylinder is 15.5 mm and the inner diameter is 12.5 mm., comprising of an overall planned wall thickness of 1.5 mm. In the image of layer 212, about 4.5 rings are seen planned for the nozzle to travel and deposit ABS. Based on the extra fine settings for the printing job in Cura, the depth of the planned layers with respect to the XY plane are 0.06 mm. Based on the results of the material separation in Acetone, it is not desirable to loose any material because it will negatively affect

tolerances and structural integrity. However, it is desirable to allow for brief material surface displacement from the Acetone and ABS reaction.

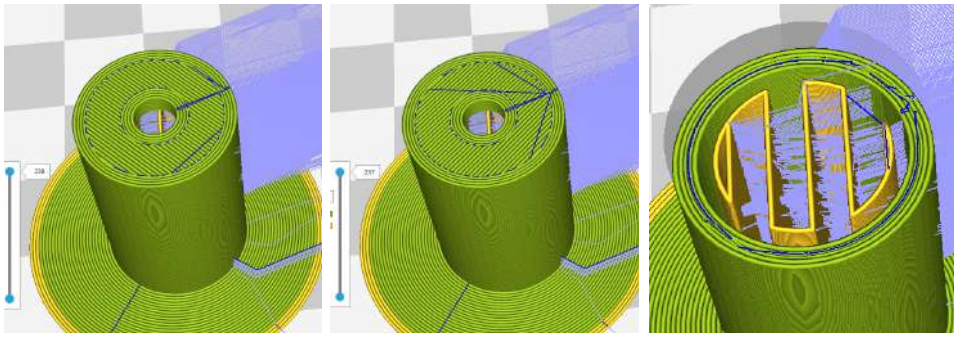

Figure 9: CAD STL Files from Cura of the Cylindrical Testing Vessels at Various Layer Depths

By visual inspection of a quick test of placing an ABS sample into a Acetone, it is obvious that a surface reaction occurs very quickly-in a matter of seconds. Based on this, a series of tests were ABS printed cylindrical vessels were printed and placed in Acetone at various time intervals. Surface finish with respect to surface roughness, was observed for the various time intervals of: 0 s, 1 s, 5 s, 10 s, 15 s, 20 s. Another goal was to print the thinnest wall possible with respect to the outer diameter of the cylinder. For this, initially the testing cylinders were printed with a wall thickness of 0.75 mm. Although the diameter of the nozzle size used was 0.4 mm, all of the prints failed (even in their ideal printing position). The prints were stopped midway and the results of the failed prints for a wall thickness of 0.75 mm can be seen in Figure 10 (a). In Figure 10 (b), a doubled wall thickness of 1.5 mm can be seen. Of seven printed cylindrical vessels, six printed without failure and one experienced similar printing failure to that of the previously tested 0.75 mm vessels. The six successful prints are displayed.

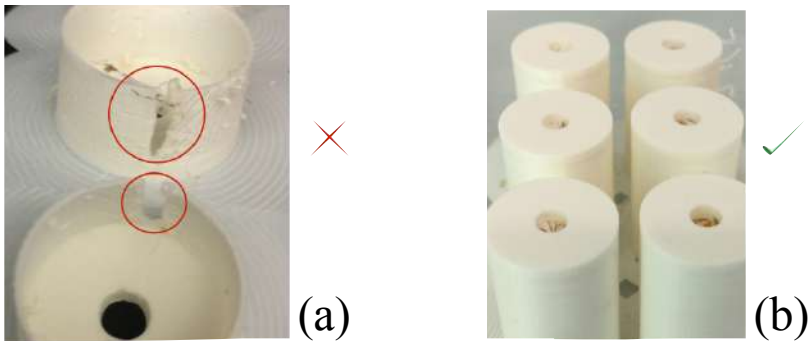

Figure 10: 3D Printed Cylindrical Vessels

A series of air pressure loss tests were conducted on the successfully printed 1.5 mm thick vessels. Each of the six cylinders were treated with an Acetone dip of different time durations ranging form 0 seconds to 20 seconds. An image of the testing specimens can be seen in Figure 11.

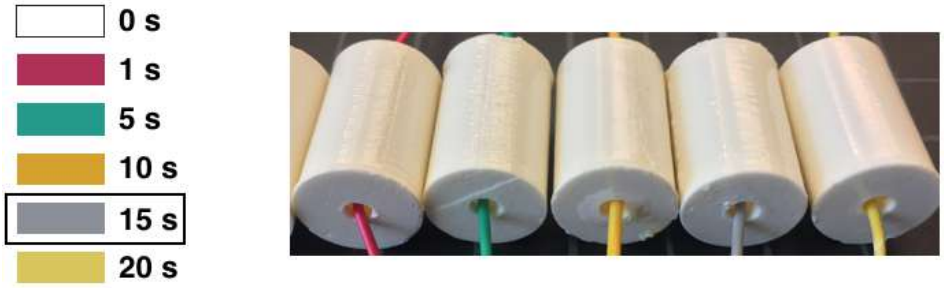

Figure 11: Treated 3D Printed Cylindrical Vessels

For the tests, one end of a cylinder was attached with tubing to a constant inlet pressure of compressed air ranging from 10 to 50 psi. At each interval of 10 psi the value of a pressure gauge also connected via tubing to the opposite end of the cylinder was recorded. The recorded values for the pressure differentials of the various combinations of treated specimens and inlet pressures can be seen in Figure 12.

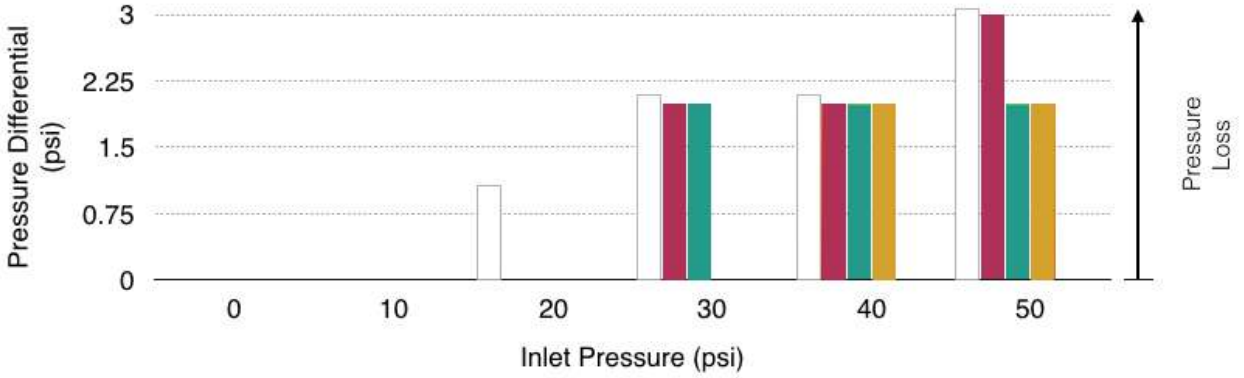

Figure 12: Pressure Differential Results for Various Treated 3D Printed Cylindrical Vessels of Wall Thickness 1.5 mm

The colors on the bar graph correspond to the previous color legend of Figure 11. Both the 15 second and 20 second chemically treated cylinders do not appear on the bar graph due to their lack of pressure loss. For this reason, the 15 second treatment was selected as the most ideal due to its minimal treatment time as well as its surface roughness. Comparing images can be seen of both the untreated sample as well as the 15 second treated sample. In figure X (a), an image of the untreated sample can be seen. When the image is edited to have a contrast of +50% and saturation of -100%, the defects of the print and deposited layers are pronounced (Figure 13, b). The surface of the cylindrical vessel treated with 15 seconds of Acetone liquid exposure can be seen in Figure 13 (c) along with its equally edited as before image in Figure 13 (d).

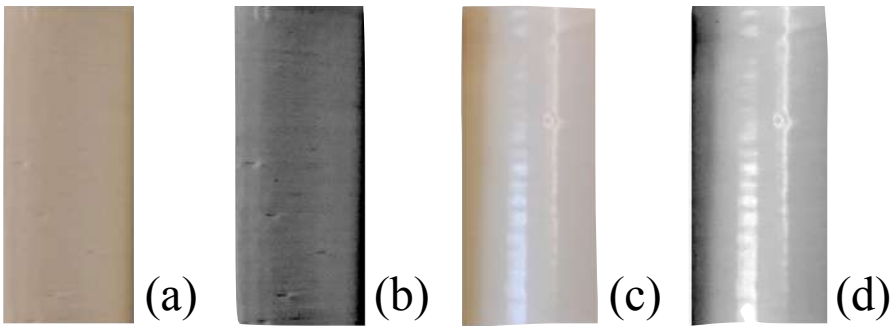

Figure 13: Surface Images of the Untreated and the 15 s Treated Testing Samples.

Final chemical processing of the printed A3 Actuator assembly parts (Figure 14 (a)) using a 15 second acetone dip treatment can be seen in Figure 14 (b).

Figure 14: Images of the Untreated and the 15 s Treated Parts

Part Bonding

For the bonding of 3D printed, ABS parts, an acrylic based adhesive was used [13]. Due to the ABS also being acrylic based (Acrylonitrile Butadiene Styrene), together with an acrylic based adhesive (Ethyl Cyanoacrylate), true surface bonding of the parts takes place. Some adhesive advantages versus other methods of bonding 3D parts such as spot welding or slurries are: (1)distribute loads/stresses evenly, (2) resist flex and vibrational assemblies, (3) form a seal as well as a bond, (4) barely increase mass of assembly, (5) virtually no change in part dimensions or geometry, (6) quickly and easily bond heat-sensitive materials. However, while

adhesive for this application had many advantages, it also had a few challenges that needed to be address in continuing with the fabrication of the 3D printed linear actuators. Cyanoacrylate adhesives do not bond well to smooth surfaces, therefore, all of the surfaces that needed to be bonded in the final actuator assembly were left without sanding. Also, Acetone acts as a solvent to cured Cyanoacrylate. This decided the order of operations for post-processing the ABS printed parts, placing all Acetone treating before the Cyanoacrylate was applied for bonding of the parts. An image of the Cyanoacrylate based adhesive used for bonding as well as the final fully assembled and bonded actuator can be seen in Figure 15 (a) and (b), respectively.

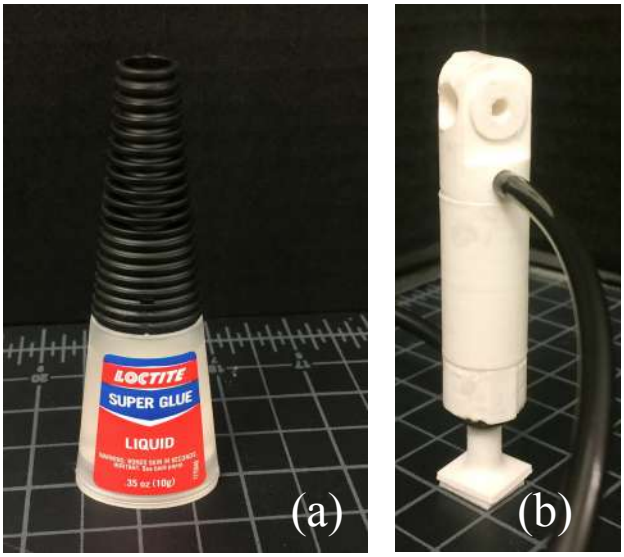

Figure 15: Images of the Bonding Adhesive as well as the Fully Assembled and Bonded Actuator

Piston Head Design

The piston head seal was designed as a dynamic, concentric application.

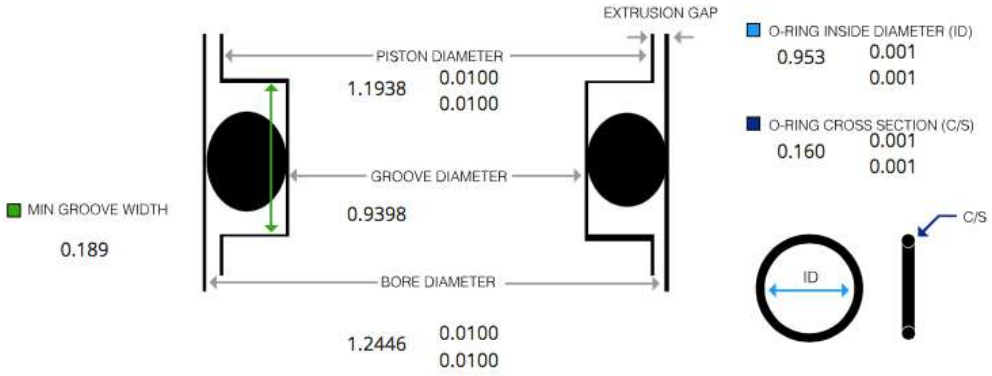

Figure 16: Schematic of a Design for the O-ring Gland for the Piston Head [8]

The % compression is the difference between the original O-ring cross-section before installation and the final cross-section after installed. It is also known as the "compression squeeze". Such a transformation can be seen in Figure 17.

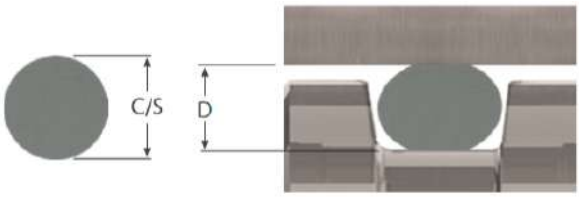

Figure 17: Schematic of Compression Squeeze

The cross-section squeeze can be calculated as a percentage with the following equation:

Cross-section squeeze % = [(Compression Squeeze)/ (C/S)]x100……(eq.2)

Three of the designs were printed with the 3D printer and tested in actuators. Design #3 was selected as the optimal design based on its % compression value of 4.8 % (nominal). During O-ring design, a stretch greater than 5% is not recommended due to the loss of seal compression that will occur [7]. Design #3 falls just below the 5% recommended threshold, adding an effective seal between the piston head and the wall of the cylinder.

Table 2: Calculated Values for Four O-ring Designs for the Piston Head

	Design #1	Design #2	Design #3	Design #4
Groove Diameter (cm)	0.9906	0.9652	0.9398	0.9144
% Compression (nominal)	20.6	12.7	4.8	0
Extrusion Gap (cm) (nominal)	0.0254	0.0254	0.0254	0.0254
% Stretch (nominal)	4.0	1.3	0	0
Squeeze (cm) (nominal)	0.03302	0.02032	0.00762	0.00508
Minimum Groove Width (cm)	0.077	0.18034	0.16764	0.15748

The selected O-ring design can be seen fabricated in Figure 18 (a) and (b). Image (a) is a top view of the piston head with the selected O-ring, and (b) is the front view of the piston head with O-ring and rod assembly.

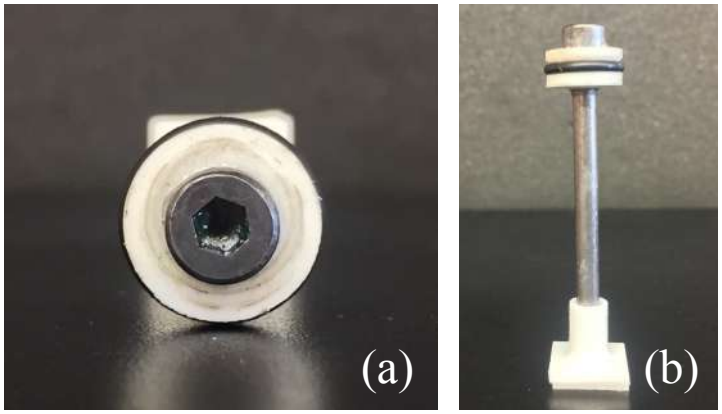

Figure 18: Images of the Selected O-ring Design, Implemented with the Piston Head Fabricated Design

Piston Rod

A galvanized steel rod was used for the piston rod (Figure 18 (b)). The particular part was selected as it is a readily available bolt at local hardware distributors. A metallic part was also very desirable for the design as it experiences many of the compressive forces during during actuation. Although the galvanizing process does not add structural improvement of the steel, it does provide a corrosive surface to chemicals or lubricants. Due to the manufacturing process of the rod, it also has a very uniform diameter throughout, overall reducing both friction and air-loss with the end cap of the actuator assembly.

The overall piston rod assembly that was used in the final actuator prototype, was selected from four experimental designs.

The first design, was possible due to the nature of the particular FDM printer used. The printer used allows for printing processes to momentarily be paused with the push of a button. When the button is pushed once more, the part will continue to be printed right where it was left off. By using this feature, enough time was provided to strategically place one of the galvanized steel rods into a couple of CAD drawn parts with supports. The experiments were performed in search of a successful printing orientation of a “piston head” that would support the placement of the steel rod. Two orientations were tested, horizontal (0 degree part orientation) and vertical (90 degree part orientation), yet only one proved to be supportive of the embedding.

Images of the horizontal embedding, with a failed result can be seen in Figure 20. The failure can be attributed to the moment that after the bolt was placed by hand (Figure 19) into the printed piston head half structure (Figure 20 (b)), the heated and planar moving nozzle impacted the protruding head of the steel bolt and simply knocked it onto the glass bed.

Figure 19: Image of Placement Process

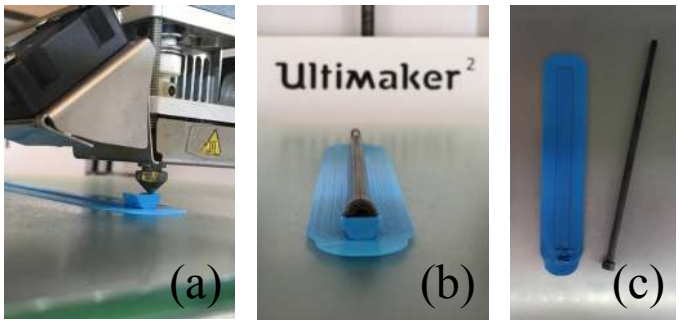

Figure 20: Images of Horizontal Part Embedding

For the case of the vertical experiment, successful embedding was dependent on the rod (with head) being placed at a very particular moment. The smaller diameter portion of the bolt, or the rod, was inserted into a slightly larger hole in the center of the printed plastic head. It was inserted after the cylindrical walls of the plastic head were printed so that none of the metallic rods larger diameter head would be protruding. Since both of the rod's head and the plastic head were flush at this moment, new plastic was able to be printed evenly on top of the metallic rod's head, therefore fully enclosing it within the printed plastic head (Figure 21 (b)). The final and successful embedding assembly (piston rod assembly design #1) of the two parts can be seen in Figure 21 (c) once all of the vertical supports were removed. Overall, design #1 for the piston rod assembly: was composed of a 3 part assembly, include 2 different materials, had a 3 hour printing time, and required a 5 minute manual assembly. It should be noted that Design #1 was printed using an Ultimaker 2 FDM 3D printer.

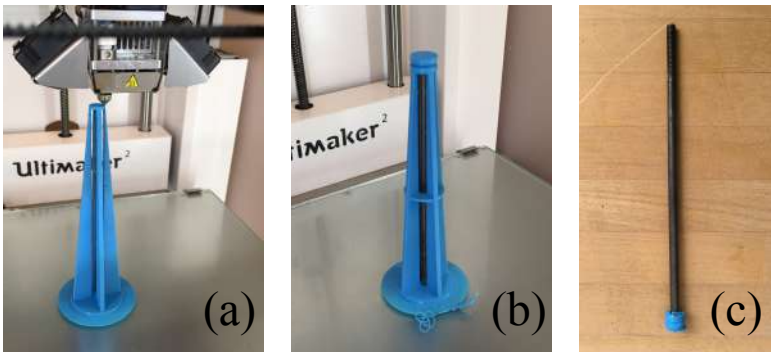

Figure 21: Images of Vertical Part Embedding and Piston Rod Assembly Design #1

The second design for the piston rod assembly consisted of: a four part assembly, 3 different types of materials, required a 20 minute printing time, and 15 minutes to assemble. A flat rubber disk was cut using a mechanical press. An image of the second design can be seen in Figure 22.

Figure 22: Images of Piston Rod Assembly Design #2

A third highly experimental design was accomplished majorly in part by the dual core printing capabilities of the used printer. The printer had the capability to print with two different materials that were extruded from two different nozzles. This design was fabricated after having learned about chemically post-processing ABS plastic (which will be later discussed in the following section). A single printed part, the piston rod design consisted of the 2 printed materials- Acrylonitrile Butadiene Styrene (ABS) and and Polylactic Acid (PLA). The supporting

base and rod were printed with layer depositions of PLA, then a number of ABS layers were printed to be used as a rubber seal once chemically processed. To firmly hold the ABS layers in place, additional layers of PLA were printed and were continuously connected to the lower layers of PLA below the ABS layers. The printing time was close to an hour for the part, required 20 minutes of sanding by hand, and an additional 20 minutes of soaking in a chemical bath. The part was soaked in a chemical that reacted with only the ABS plastic, transforming it from rigid to elastic. Images of the part can be seen in Figure 23 before, during, and after post-processing. Once processed, the ABS portion of the print became rubberized, while the rest of the part remained rigid. This allowed for a similar functioning part, that if refined, could possibly replace the previous design assemblies.

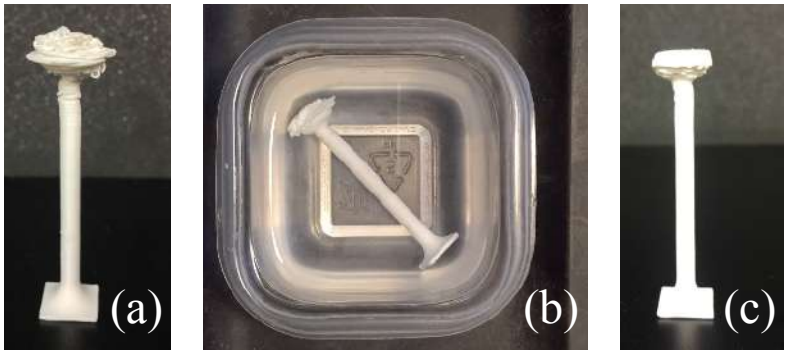

Figure 23: Images of Piston Rod Assembly Design #3 Pre and Post-Processing

A fourth design for the piston rod assembly was realized and ultimately yielded the greatest working results for the designed actuator. The four part assembly, with three different materials including steel, ABS plastic, and rubber, had a printing time of 30 minutes and was assembled in 15 minutes. When tested, this design was reliable and easily repeatable when fabricating multiple prototypes. An image of the design is shown in Figure 24. Further design details were also presented in the previous subsection, “Piston Head”.

Figure 24: Image of Piston Rod Assembly Design #4

Piezoelectric Sensor Fabrication

A piezoelectric sensor was fabricated and used during testing of the A3 Actuator. It was used as a force sensor and was fixed to the bottom of the actuator. To be used a force sensor, the parameters of the piezoelectric material first needed to be determined. Two values were measured of the piezoelectric crystal- the piezoelectric coefficient and capacitance. The piezoelectric coefficient was measured with a piezo meter and can be seen in Figure 25 (a) and the capacitance was measured with a multimeter (Figure 25 (b)). The values measured were C= 0.5 nF for the capacitance and d=365 pC/N for the piezoelectric coefficient.

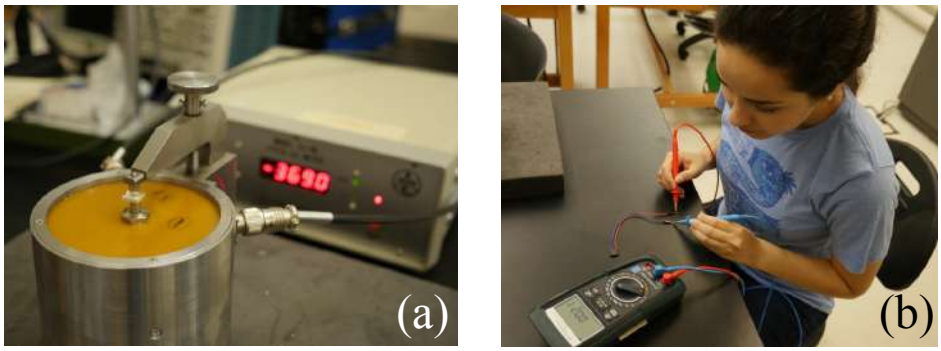

Figure 25: Images of the Piezoelectric Crystal Measurements

The sensor was fabricated using a square piezoelectric crystal sample, measuring 1 cm x 1cm and was 0.2 cm thick (as seen in center of Figure 26). The copper electrodes sheets were carefully adhered to either side of the piezo using a high conductivity silver epoxy.

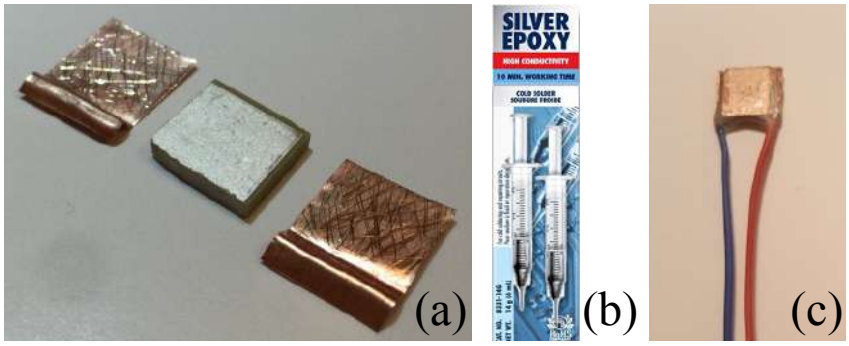

Figure 26: Images of the Piezoelectric Crystal (Center) with Two Copper Electrode Sheets, Silver Epoxy, and Composite Sensor Structure

To calculate the resulting forces, the varying voltages were found using voltage readings from an Arduino code running during actuator testing and input into the equation [11]:

$$F = CV/d \quad \text{(eq. 3)}$$

For the equation, F is the force produced upon deformation of the crystal, C is the capacitance measured for the crystal, d is the piezoelectric coefficient also measured for the crystal, and V is the varying voltage output from the crystal to the microcontroller.

The circuit that was used for testing the piezoelectric sensor can be seen in Figure 27.

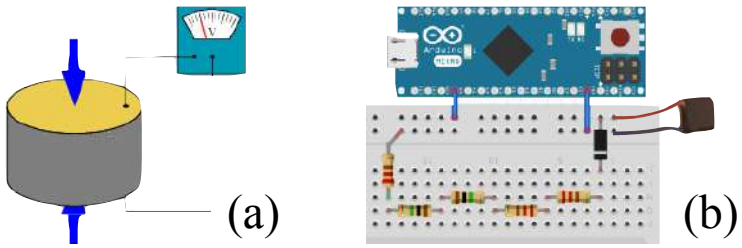

Figure 27: Piezoelectric Sensor Principle Figure and Circuit Schematic for the Piezoelectric Sensor

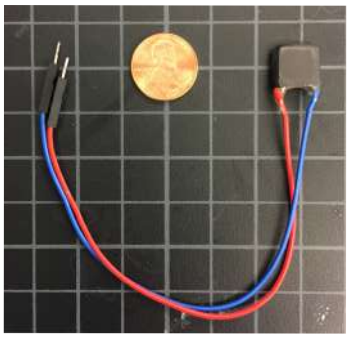

Figure 28: Image of Final Fabricated Piezoelectric Sensor

Final Working Assembly

The final assembly of the 3D printed actuator, A3, is shown in Figure 29 (a), (b), and (c) with an isometric view, front view, and a view scaled with a penny. The final assembly used for testing was given a square, flat surfaced base that was adhered to the steel piston rod. This flat base provided upright support for the actuator and distributed forces more evenly to the piezo sensor.

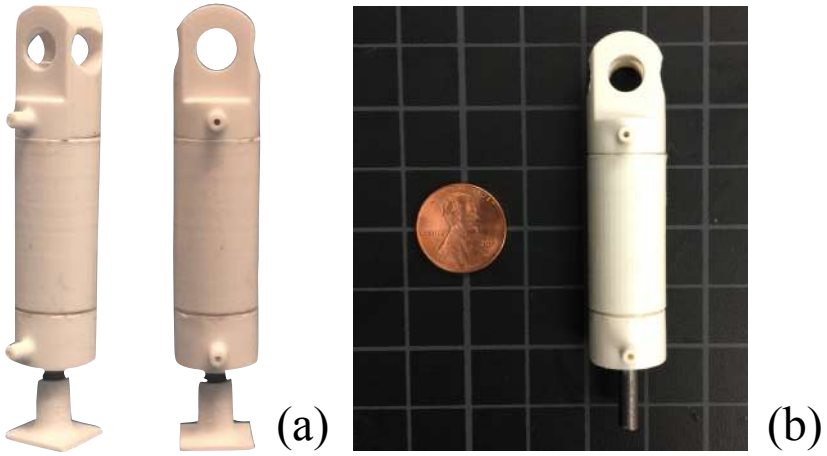

Figure 29: Views of the Final Assembly of A3 Actuator

Summary of Failed Actuator Prototypes

Over the course of the thesis work, many prototypes were fabricated (Figure 30) and few were successful. Success of a prototype actuator was found when many variables were

considered such as: material selection, post-processing of plastic, design tolerances and tolerances of the machine used, assembly fits and bonds, internal friction of the cylinder, lubricant selection and amount, increased internal stresses produced by the selected orientation of print, and fillets added for the support of external connection ports.

Figure 30: Image of Failed Actuator Prototypes

CHAPTER THREE: EXPERIMENTAL SETUP

Experimental Setup

For experimental testing, the hardware components were set as shown in Figure 31.

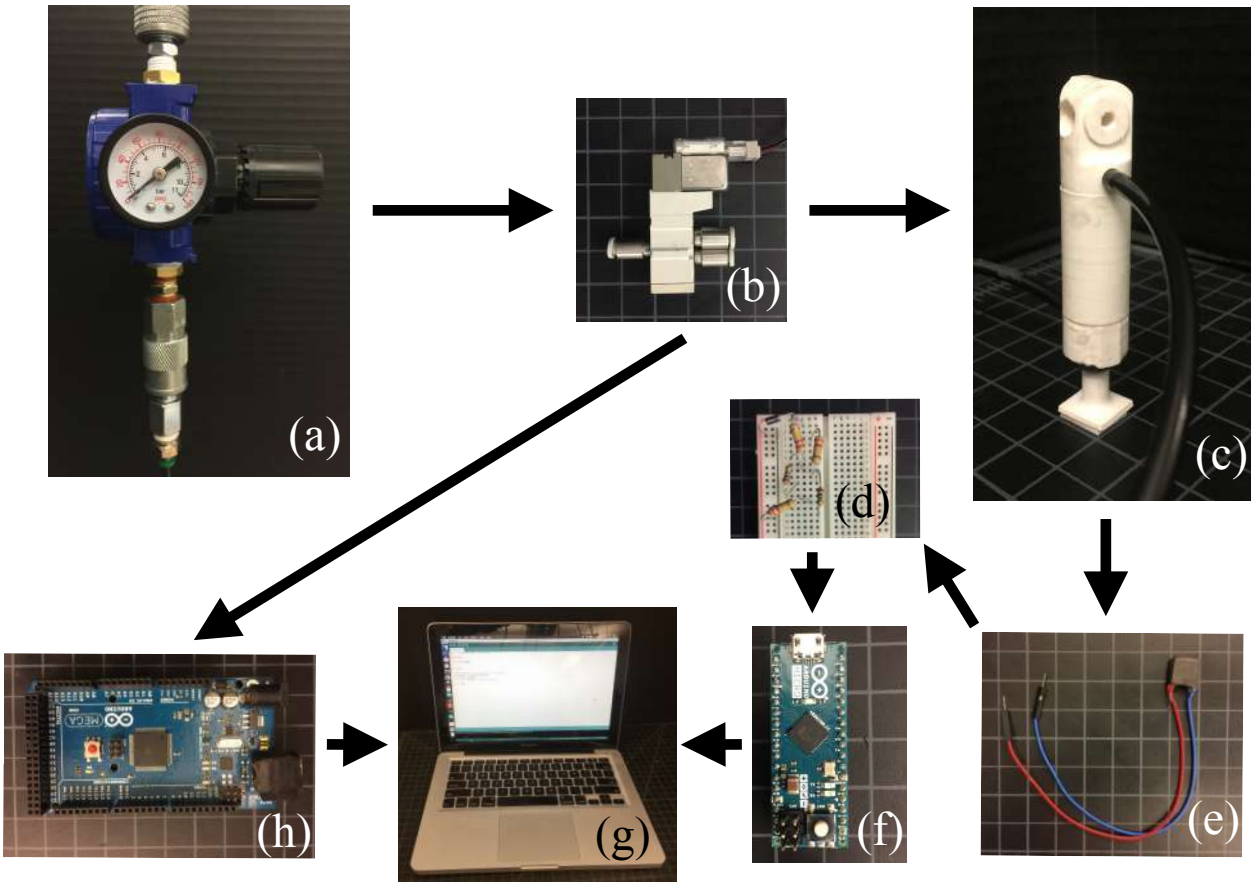

Figure 31: Final Experimental Setup Hardware Components used for Testing

Figure 31 (a) shows the compressed air hose connected to a manual valve with a pressure gauge, this is then connected to fittings that proved a feasible connection to the 4mm outer diameter pneumatic tubing. The tubing is then connected to a double-acting solenoid valve (b) with three ports. The single port on the left side of the image (b) is connected directly to the compressor air inlet, while the other two ports are connected to port a and port b of the 3D printed actuator (c). On the bottom of the actuator, a protected piezo sensor (e) is connected to

the bottom base of the piston rod. The red lead in (e) is connected to the positive terminal of the breadboard (d), while the blue lead is connected to the negative terminal of the breadboard (d). The lead is run from the breadboard circuit (d) to an analog pin of the Arduino micro and is then connected to a computer. The computer (g) reads and saves the varying voltage signal produced from the piezoelectric sensor as it deflects under the solenoidal movement of the double-acting actuator. The actuators up and down movement is controlled by the Arduino mega (h), which also acts as a power source for the ON-OFF double-acting solenoid.

Determining Solenoid and Actuator Timing

Timing for the solenoid was determined by iterative testing of the ON-OFF time delays within the Arduino program. Once the A3 actuator was attached to the experimental setup, a number of time delays were tested from 0.1 s to 2.0s. The successful time delay (Table 3) for the actuator to achieve a full instroke and outstroke was a one-way delay of 0.1 s. The time delay was deemed successful based on the achievement of a full instroke of the rod while the actuator was at its overall peak vertical displacement. The process is seen in Figure 32 (a), (b), and (c).

Time Delay (s) to travel 1 Stroke Length	Successful Stroke
2.0	N
1.75	N
1.5	N
1.25	N
1.0	N
0.75	N
0.5	N
0.25	N
0.15	N
0.1	Y

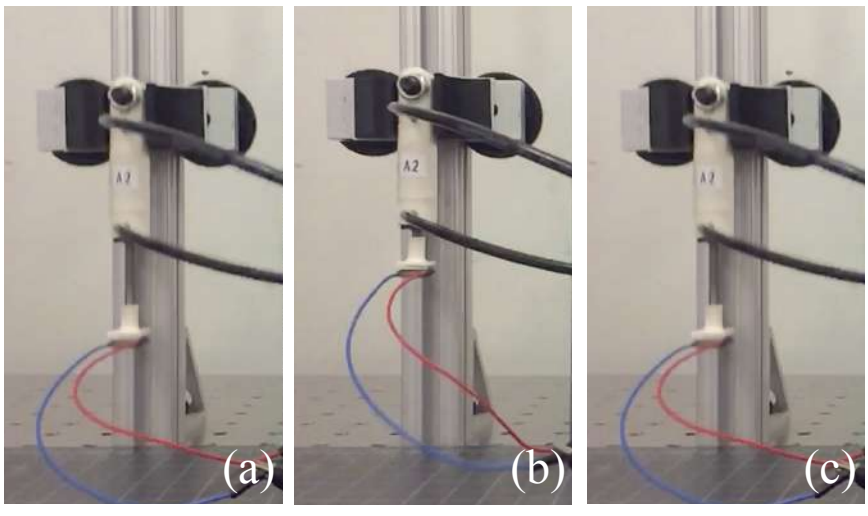

Table 3 and Figure 32: Timing Experiment to Determine the Timing for the Actuator

Calibrating the Piezoelectric Sensor

The fabricated piezoelectric sensor sent ADC values to the micro and converted the values into output voltages using the two commands, “int piezo1 = analogRead(PIEZO_PIN1);” and “float piezo = (piezo1 / 1023.0*5);”. These values were printed in increments of 0.05 s.

Determining Actuator Operating Pressure

Theoretical stresses were calculated as basis for selecting operating internal air pressures for the testing of the actuator prototypes. The circumferential and longitudinal stresses were calculated using equations 4 and 5 for a pressurized cylinder with respect to yield stress.

$$\sigma_1 = pr/t \quad \text{.....(eq. 4)}$$

$$\sigma_2 = pr/2t \quad \text{.....(eq. 5)}$$

These types of stresses can be seen in the following figure X.

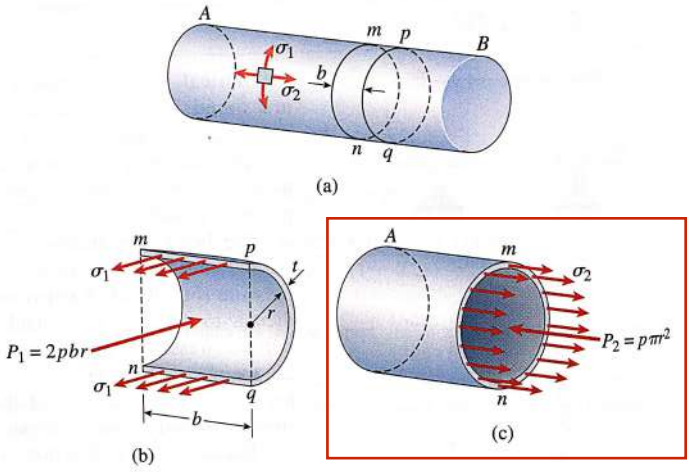

Figure 34: Stress Induction within a Pressurized Cylinder [15]

The yield stress used for the calculations was selected from a study that examined the tensile, compressive, and flexural properties when ABS plastic was FDM printed at different orientations [14]. Based on five samples printed to ASTM standards, the found average yield

stress for samples printed at a 90 degree orientation (equal to the printing orientation of the cylinder used in the tested actuator) was 7.9 MPA/ 1.14 ksi.

Solving for the pressure using the circumferential stress equation yields equation 6. Also solving for the pressure using the longitudinal stress equation yields equation 7.

$$p = \sigma_1 t / r \quad \text{(eq. 6)}$$

$$p = 2\sigma_2 t / r \quad \text{(eq. 7)}$$

The calculated pressure from eq. 6 was 324.39 psi and the calculated pressure relative to the longitudinal stress was calculated to be 648.78 psi using eq. 7. These results yielded significantly higher internal pressure values then capable with the standard compressed air issued within the laboratory. The maximum available pressure of compressed air was 100 psi. Static testing of the cylinder with the actuator assembly was performed without failure up to 100 psi. Dynamic testing of an earlier prototype of the actuator assembly eventually (after about 100 cycles) yielded a failure that was transverse to the length of the cylinder. This was due to the internal longitudinal stresses overcoming the "weldments" of the FDM printing process. The exact failure mentioned can be seen in the following Figure 34. Following this test of an earlier prototype, dynamic tests were carried out with a maximum internal operating pressure of 50 psi for the preservation of the prototypes. Additional experimental dynamic tests at higher pressure were carried out between 50 psi and 70 psi for low cycle amounts.

Figure 34: Longitudinal Stress Failure of a Dynamically Tested Actuator Prototype

CHAPTER FOUR: TESTING

Test: Actuators "Hopping" with Supports

Experimental jumping tests were performed for two actuator prototypes, A2 and A3. The A2 actuator was an earlier prototype of the A3 actuator. The A2 Actuator Hopper had 4 supports to stabilize the actuator to remain in an upright position.The supports for the A2 Actuator Hopper had radii of curvature of 4.75 cm. with 90 degrees in between each of the supports. Images of the A2 actuator can be seen in Figure 35 (a), (b), (c), and (d), that include the fully extended, top, fully retracted, and bottom views, respectively.

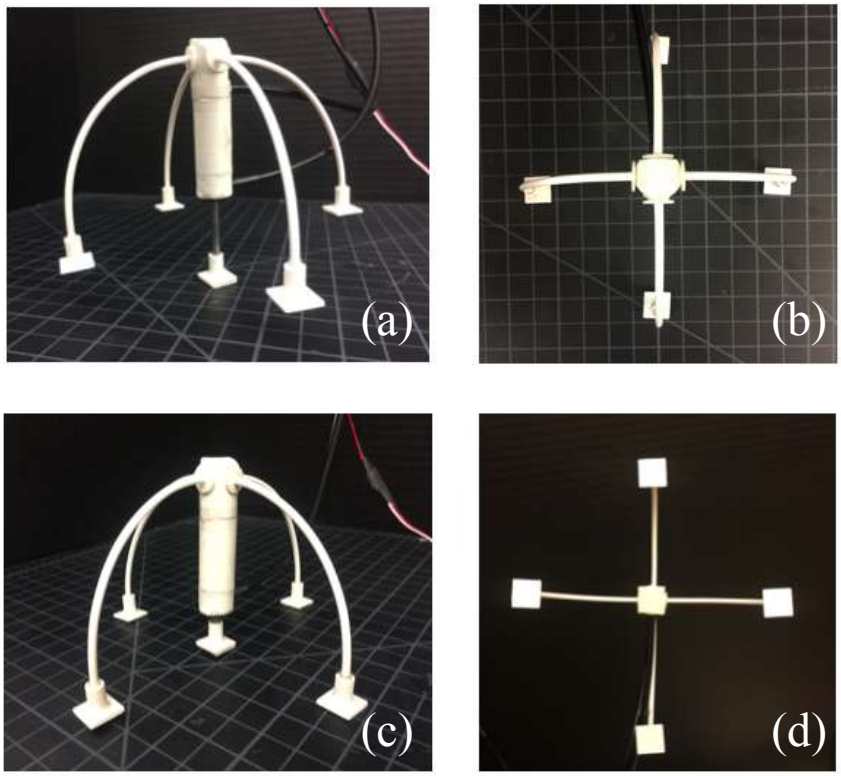

Figure 35: Images of the A2 Actuator Hopper

The A2 Hopper was found to remain stable during in place hopping and mages of the actuator lifting off to a maximum vertical displacement of in 3.0 inches can be seen Figure 39

(a), (b), and (c) with an inlet pressure of 40 psi. The hopper failed however, to remain stable when jumping from a declined plane to a flat plane (Figure 37 (a), (b), and (c)). Due to the placement of the four supports and the overall distance between the supports, the end effector of the actuator was too far from the edge of the declined plane for a successful hop onto a flat plane. The lift off was successful, however when the hopper traveled downwards, the back support made contact with the edge of the declined plane and caused the hopper to rotate in a forward and clockwise direction. Due to the rotation, the front support then made first contact with the flat plane and ultimately resulted in an unstable landing of the hopper.

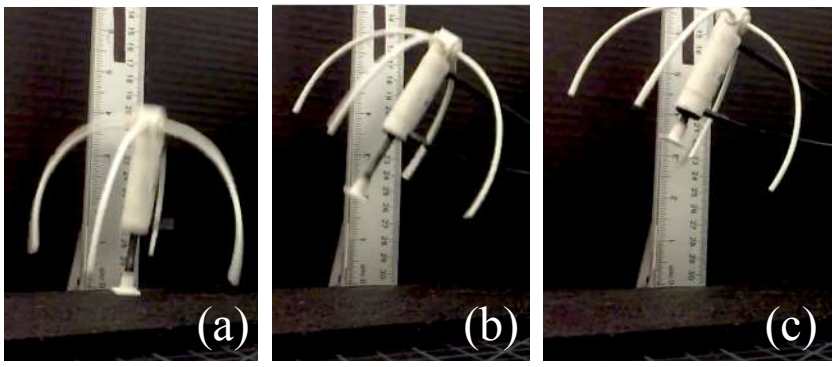

Figure 36: Images of the A2 Actuator Hopper during Successful Hop from Horizontal Plane

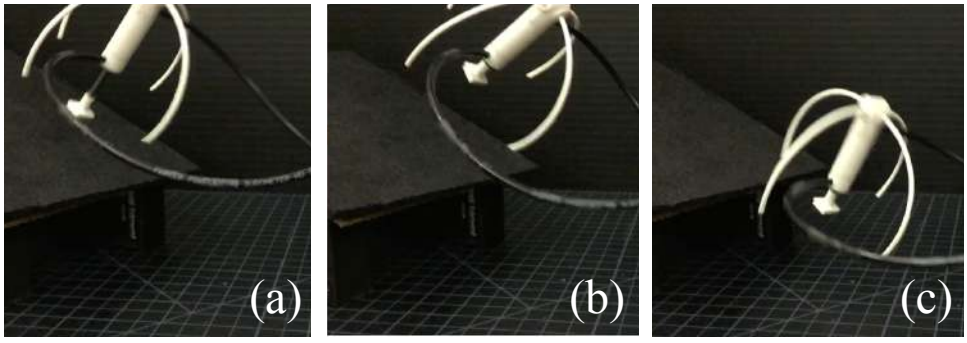

Figure 37: Images of the A2 Actuator Hopper during Failed Hop from Declined Plane

To address the issue of unstable landing from a declined plane to a horizontal plane, a new hopper was prototyped using the improved A3 actuator as well as a reduced number of

supports-three. For the top of the supports a 90 degree radial distance remained. However, for the bottom of the supports, a major increase occurred between the front two supports and the back support with a new radial distance of about 165 degrees. The front two supports were given a radial distance of about 30 degrees. The prototyped A3 Hopper can be seen in Figure 38 (a), (b), (c), and (d), that include the fully extended, top, fully retracted, and bottom views, respectively. The A3 hopper was able to successfully jump from a declined plant to a flat place while remaining upright as seen in Figure 39 (a), (b), and (c).

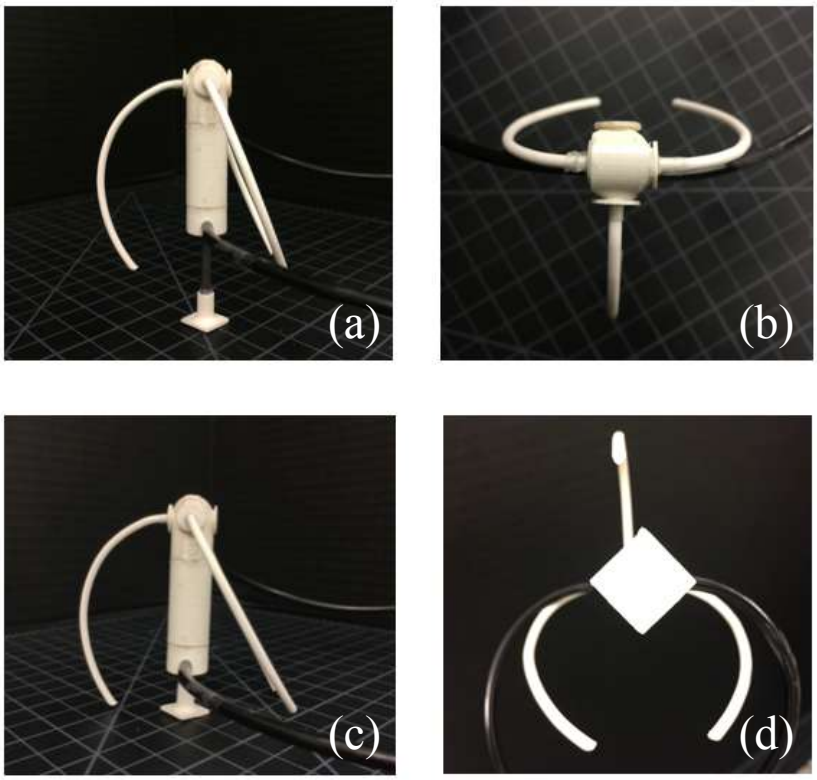

Figure 38: Images of the A3 Actuator Hopper

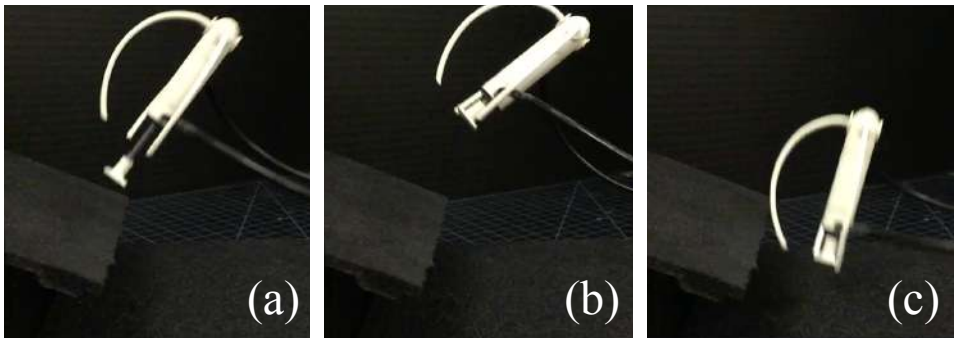

Figure 39: Images of the A3 Actuator Hopper During Successful Hop from Declined Plane

Test: Outstroke Forces for Actuators on Rails

The developed actuator, A3, was attached to a set of rollers on a vertical linear rail and tested at various inlet pressures for the measurement of outstroke forces. The same tests were performed for a commercially available double-acting linear actuator by LEGO Education. The two shared comparable dimensions. Images of the experimental setup for measuring the outstroke forces of the actuators can be seen in Figure 40 (a) and (b). The LEGO actuator was fitted to allow a similar extension length of the piston and a identical end effector to that of the A3 actuator was added to ensure similar testing conditions Figure 41.

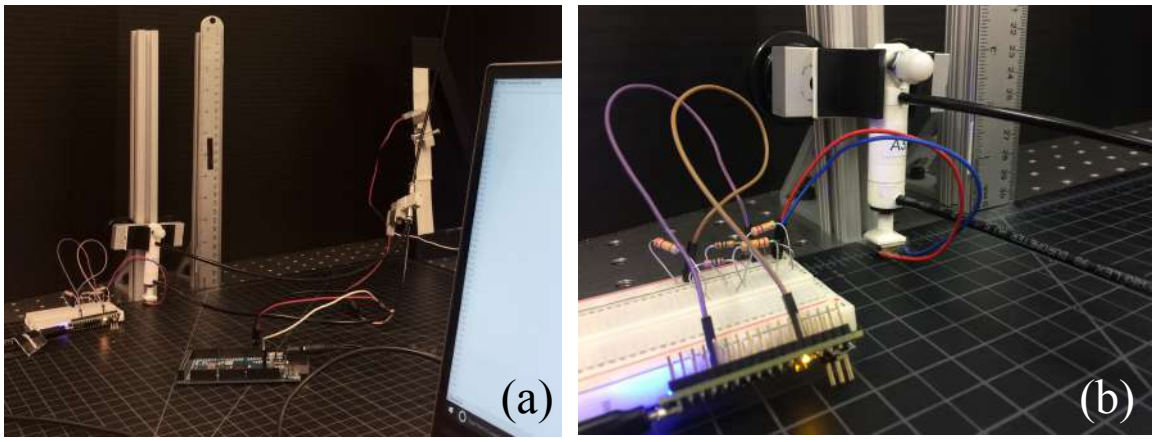

Figure 40: Images of the Experimental Setup for the Actuators on Rail

Figure 41: Images of the Fitted LEGO Actuator

The voltage values from the displacement of the piezoelectric sensor were measured and used in equation 3 to calculate the various output forces. The output force results for both actuators can be seen in the following Figures 42, 43, and 44 for input pressures of 20, 30, and 40 psi, respectively. Measurements were recorded for 30 outstroke displacements for both of the actuators and graphed in overlay. *The time intervals in between each outstroke is approximately 0.066 seconds or 66 milliseconds.

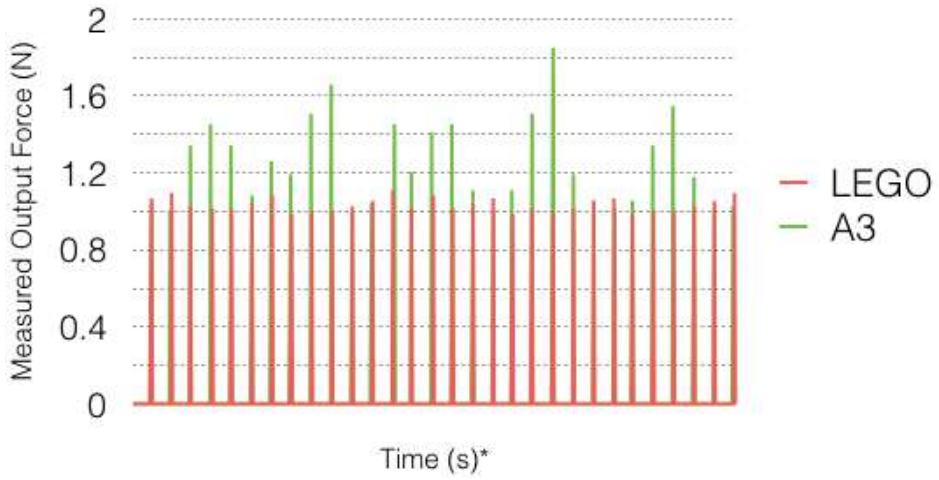

Figure 42: Measured Output Force vs. Time (s) at Inlet Pressure 20 psi

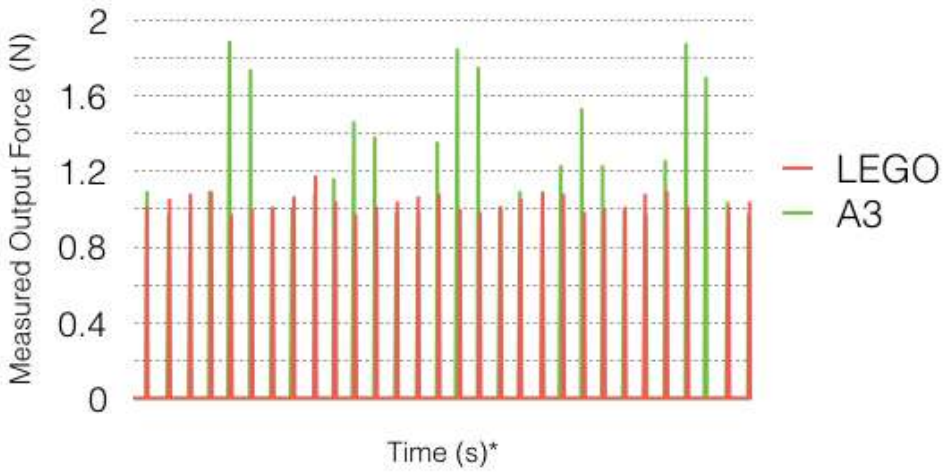

Figure 43: Measured Output Force vs. Time (s) at Inlet Pressure 30 psi

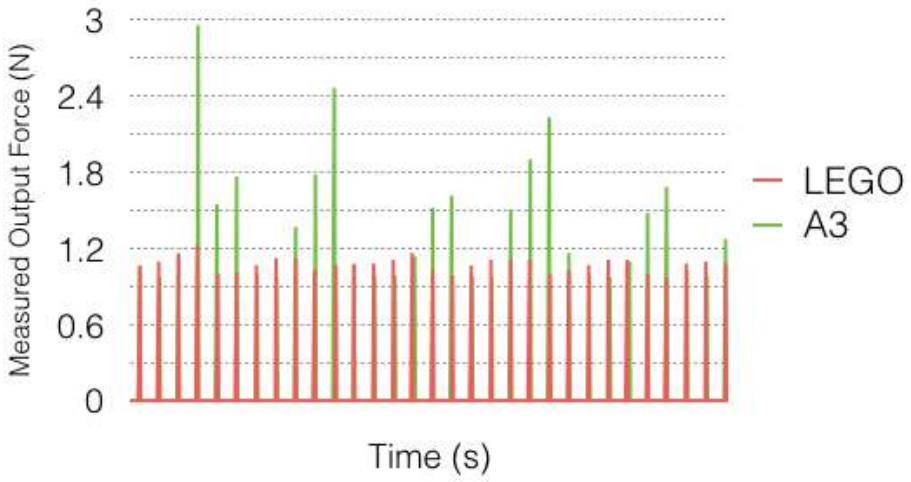

Figure 44: Measured Output Force vs. Time (s) at Inlet Pressure 40 psi

The final average calculated outstroke force results based on the voltage readings from the piezoelectric sensor are found in the following Table 4. The findings reveal slightly higher output forces from the A3 actuator when compared to the LEGO Actuator. For an inlet pressure of 20 psi there is about a 18 % difference, for 30 psi a 22 % difference, and for 40 psi there was approximately a difference of 24 %.

Table 4: Overall Outstroke Force Results for the A3 and LEGO Actuators

	$F_{average}$, (N) @20 PSI	$F_{average}$, (N) @30 PSI	$F_{average}$, (N) @40 PSI
LEGO	1.035	1.006	1.112
A3	1.248	1.261	1.421

Test: Vertical Displacements for Actuators on Rails

A series of tests were performed on the actuators to inspect achievable vertical displacements when also attached to rollers on a rail. Similar to the previous tests, the actuators were both subjected to various input pressures. An image of the experimental setup can be seen in Figure 45. The vertical displacement was measured as a result of the peak height achieved by the actuator during hop minus the starting standing height when in a fully compressed position. The reference point used for the measurements was the right end corner of the roller's metal bracket as seen in Figure 45.

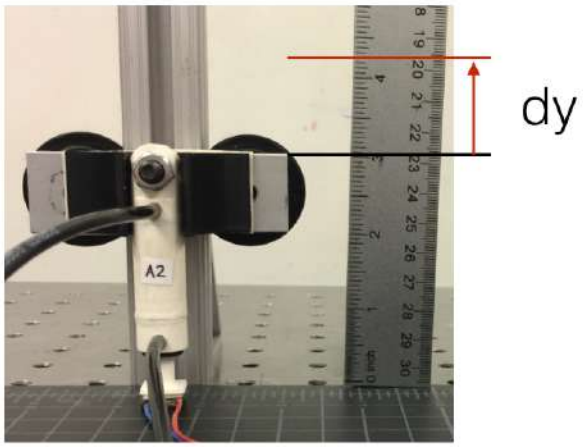

Figure 45: Diagram of the Method of Vertical Displacement

The measured vertical displacement results for both of the actuators at varying input pressures of 20 psi, 30 psi, and 40 psi can be seen in Figure 46.

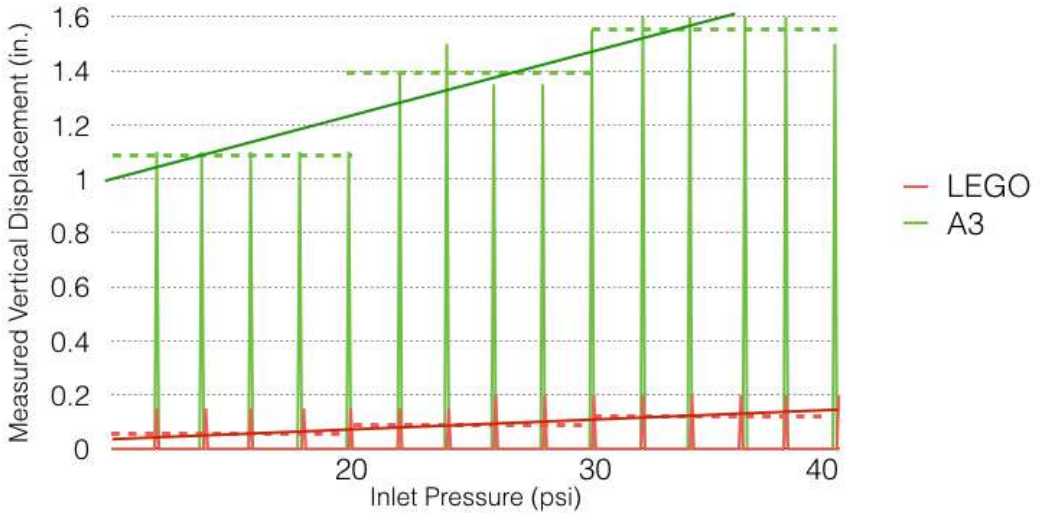

Figure 46: Measured Vertical Displacement vs. Inlet Pressure for the A3 and LEGO Actuators

The final results as seen in Figure 46 were taken to be inconclusive due to an observation of the LEGO actuator that was made during testing. While operating at higher input pressure of 40 psi, a mechanism failure of the piston head was noticed when a slow motion video was examined. Also, it was theorized that due to the design of the LEGO piston head, the LEGO actuator experienced a much higher amount of internal friction between the head and cylinder (although the cylinder was of a lesser friction than the A3 actuator cylinder) while traveling. Due to this increased internal friction, the LEGO actuator was measured to take 0.066 seconds to travel a full stroke's length, while the A3 actuator was measured to spend half the amount of time traveling nearly the same stroke length. Due to these findings, a final comparison of the two actuators with regards to vertical displacements was not made. A summary of the main findings can be found in the following Table 5.

Table 5: Results of Measured Vertical Displacement vs. Inlet Pressure

	Vertical Displacement (in) @20 PSI	Vertical Displacement (in) @30 PSI	Vertical Displacement (in) @40 PSI	Stroke Length (in)	Time to travel 1 outstroke length (s)
LEGO	< 0.05	< 0.1	< 0.2 (Piston seal failure?)	0.87	0.066
A3	1.1	1.4	1.55	0.79	0.033

CHAPTER FIVE: COMPARISON OF A3 ACTUATOR WITH COMMERCIALLY AVAILABLE ACTUATORS

"Hobby Grade", "Hobby Printed", and "High End" Actuators

The actuators compared in this chapter were placed into subgroups. The LEGO linear pneumatic actuator was considered a "Hobby Grade", professionally fabricated, commercially available actuator. A Faulhaber Series DC rotary micromotor and Bimba linear pneumatic actuator were both considered to be "High End", professionally fabricated, and commercially available actuators. Finally, the A3 Actuator was considered a "Hobby Printed", experimental actuator, with the performance in between that of the "Hobby Grade" and "High End" actuators. The compared actuators can be seen in the following Figure 47 including the: (a) LEGO Education linear pneumatic actuator, (b) A3 linear pneumatic actuator, (c) Faulhaber Series 1219 G DC rotary micromotor, and the (d) Bimba 01-DP linear pneumatic actuator, respectively.

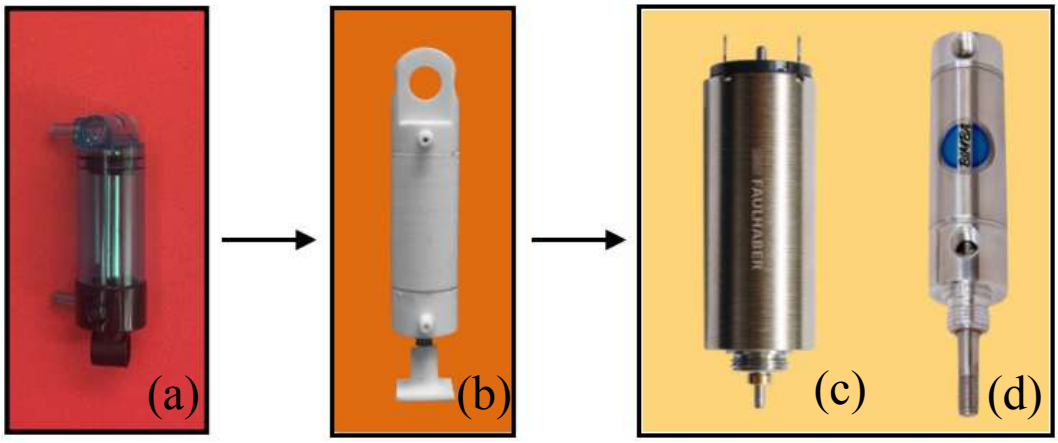

Figure 47: Comparing Various Commercial Actuators and the A3 Actuator

A diagram was created to display the relative sizes of the actuators with respect to the outer cylinder diameters and the overall lengths of the actuators. The results can be seen in the following Figure 48.

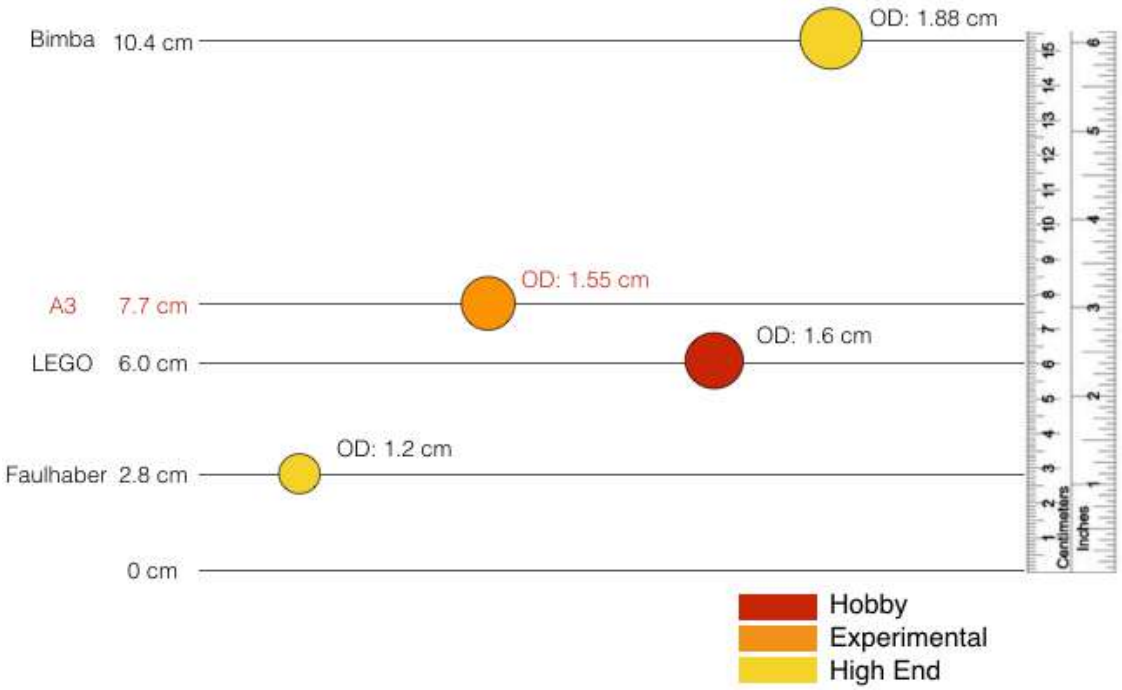

Figure 48: Scale of Various Compared Actuators

A table of the relevant dimensions, material make, and actuator type for the compared actuators can be seen in Table 6. Average power outputs, pressure ratings, and theoretical outstroke forces were calculated for the actuators with sufficient information. These results can be seen in Table 7.

Table 6: Dimensions of Compared Actuators

Actuator	Actuator Type	Compressed Length (cm)	Stroke Length (cm)	Cylinder Bore (cm)	OD (cm)	Wall thickness (cm)	Materials	Mass (g)
Lego	2-Way, Linear, Pneumatic	6.0	2.2	1.4	1.6	0.15	ABS Plastic/ Polycarbonate	10
A3	2-Way, Linear, Pneumatic	7.7	2.0	1.23	1.55	0.16	ABS Plastic/ Steel	12
Faulhaber Series 1219...G	DC Rotary Micromotor	2.785	—	—	1.2	?	Steel/Nickel plated	11
Bimba 01-DP	2-Way, Linear, Pneumatic	10.9	2.54	1.11	1.88	?	Stainless steel/ Aluminum	45.4

Table 7: Performance Metrics of Compared Actuators

Actuator	Average Power Output (W) @40 psi	Pressure Rating (PSI)	Theoretical Outstroke Force* @ 40 psi (N)
Lego	? (experimental)	TBD	52.5
A3	1 (experimental)	TBD	32.7
Faulhaber	2	-	-
Bimba	?	250	26.7

Interestingly, the theoretical outstroke force was also calculated using equation 1 which is dependent on a fixed input pressure, and varied cross sectional areas of the cylinders. The linear pneumatic actuator calculated to have the greatest output force was the actuator that actually produced the least. This is proof that many variables in the design process of linear pneumatic actuators must be taken into account in order to achieve performance results similar to those calculated with theoretical equations.

CHAPTER SIX: ACTUATOR IMPLEMENTATION IN A ROBOT

Pixar's Luxo Jr. Lamp

A prototype of the actuator was implemented into a 3D printed robotic prototype (Figure 51) of Pixar's famous Luxo Jr lamp (Figure 49). The lamp was drawn and assembled in SolidWorks (Figure 50) .

Figure 49: Image of Pixar's Luxo and Luxo Jr.

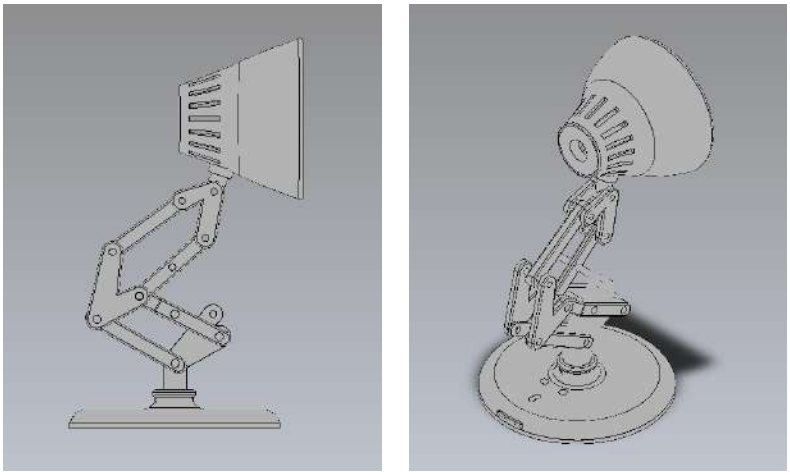

Figure 50: Image of CAD Assemblies in SolidWorks of Luxo Jr. Lamp Prototype

Figure 51: Image of CAD Luxo Jr. 3D Printed Lamp Prototype

Hardware testing was performed with the lamp and implemented actuator at an inlet pressure of 30 psi. The results can be seen in the following images in Figure 52.

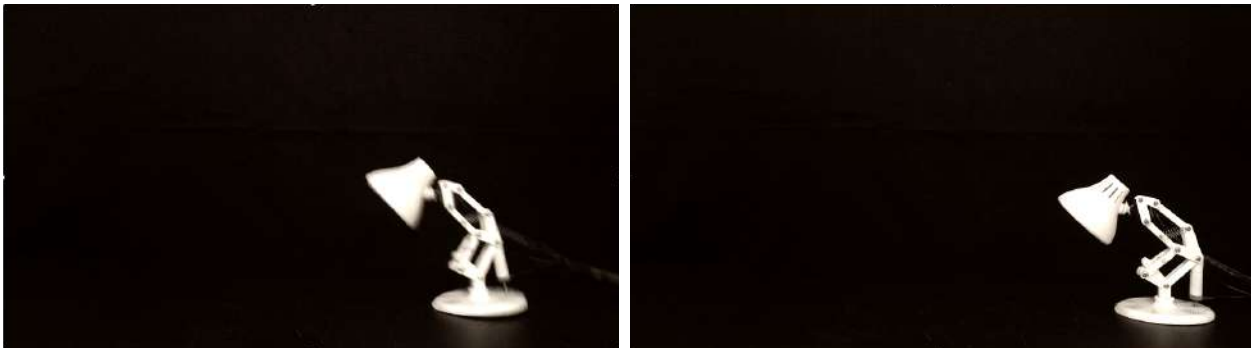

Figure 52: Images of Lamp Robot with Implemented A3 Actuator

Dynamic Modeling was done in Matlab's Simscape to explore various spring combinations for the improvement of the prototype. Screen images can be seen in Figure 53. Simscape is a very useful program to test for the dynamics of robotic systems and can be used with the CAD files of the A3 Actuator to further test its implementation. The current lamp robot can be scaled, modified, and paired with an also scaled or modified actuator to test within the Simscape environment before fabricating new prototypes.

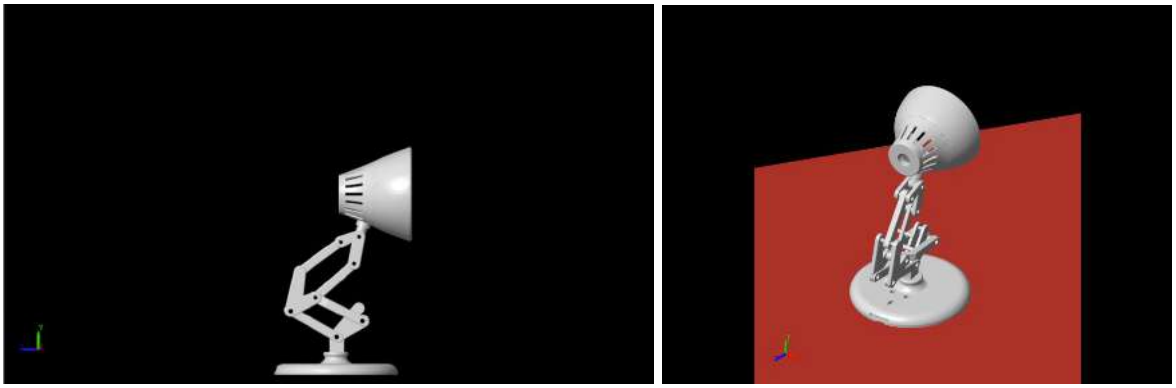

Figure 53: Image of CAD Luxo Jr. Prototype in Matlab's Simscape

CONCLUSION

In summary, it was found that 3D printed pneumatic actuators are possible to fabricate with hobby grade 3D printers and can yield comparable performance results to that of high-end commercial actuators of similar size. A benefit of 3D printed pneumatic actuators is that they combine the high power of pneumatics with the low weight of plastics and can have added strength structurally through selective placement of metal parts. Such actuators are proven in this thesis to be promising for robotic applications. The final developed A3 Actuator can be seen in the following figure (Figure 54) along with its characteristics in Tables 8 and 9.

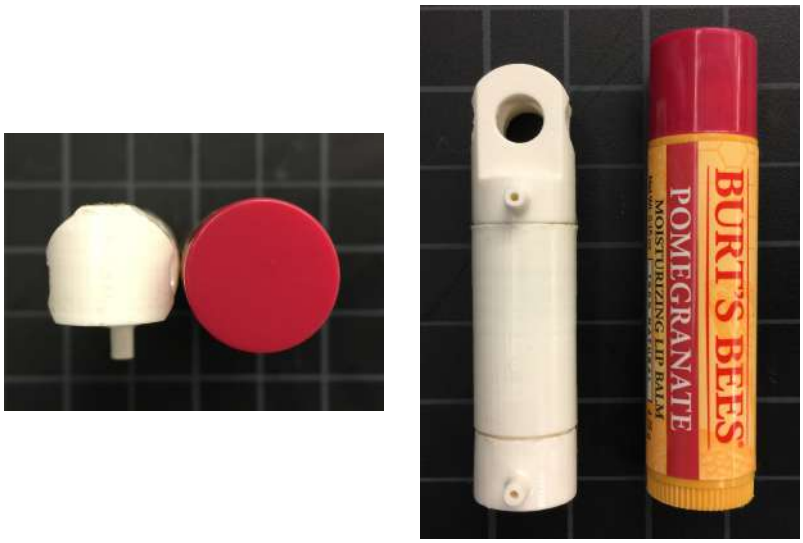

Figure 54: Final A3 Actuator Compared in Size to a Lip Balm

Table 8: A3 Actuator Dimensions

Compressed Length (cm)	Stroke Length (cm)	Cylinder Bore (cm)	OD (cm)	Wall thickness (cm)	Materials	Mass (g)
7.7	2.0	1.23	1.55	0.16	ABS Plastic/Steel	12

Table 9: A3 Actuator Performance Summary

Peak Power Output (W) @40 PSI	Static Pressure Rating (PSI)	Theoretical Outstroke Force* @ 40 PSI (N)	Measured Outstroke Peak Force @ 40 PSI (N)	Speed of Extension (s) @ 40 PSI	Vertical Displacement (cm)
2	100	32.7	3.0	0.033	4.0

REFERENCES

[1] Patent US2293167 - Hydraulic cylinder. (n.d.). Retrieved December 08, 2017, from https://www.google.com/patents/US2293167

[2] Patent US3023739 - High speed pneumatic actuator. (n.d.). Retrieved December 08, 2017, from https://www.google.com/patents/US3023739

[3] Patent US3202062 - Actuator. (n.d.). Retrieved December 08, 2017, from https://www.google.com/patents/US3202062

[4] Pneumatic Actuator (Air Cylinder) Basics. (2017, October 30). Retrieved December 08, 2017, from https://library.automationdirect.com/pneumatic-actuator-air-cylinder-basics/

[5] Wong, K. V., & Hernandez, A. (2012, January 01). Directory of Open Access Journals. Retrieved December 08, 2017, from https://doaj.org/article/ef9087cafc7a4b25bbd6317e7dab9391

[6] Ultimaker 3 specifications | Ultimaker. (n.d.). Retrieved December 08, 2017, from https://ultimaker.com/en/products/ultimaker-3/specifications

[7] Hi-Tech Seals Inc. (n.d.). Retrieved December 08, 2017, from http://www.hitechseals.com/

[8] O-Ring Gland Calculatr. (n.d.). Retrieved December 08, 2017, from http://www.applerubber.com/oring-gland-calculator/

[9] ABS plastic. (n.d.). Retrieved December 08, 2017, from https://www.interstateplastics.com/ABS-sheets-rods.php

[10] Polymer Guide: If you seek solvation. (2015, April 21). Retrieved December 08, 2017, from http://depts.washington.edu/open3dp/2015/01/polymer-guide-if-you-seek-solvation/

[11] (n.d.). Retrieved December 08, 2017, from http://www.piezo.com/tech1terms.html

[12] Rodríguez, J. F., Thomas, J. P., & Renaud, J. E. (2001). Mechanical behavior of acrylonitrile butadiene styrene (ABS) fused deposition materials. Experimental investigation. *Rapid Prototyping Journal, 7*(3), 148-158. doi:10.1108/13552540110395547

[13] Kenneth Korane | Jun 15, 2000. (2016, April 07). Guidelines for Bonding Plastics. Retrieved December 08, 2017, from http://www.machinedesign.com/adhesives/guidelines-bonding-plastics

[14] Hernandez, R. (n.d.). ANALYZING THE TENSILE, COMPRESSIVE, AND FLEXURAL PROPERTIES OF 3D PRINTED ABS P430 PLASTIC BASED ON PRINTING

ORIENTATION USING FUSED DEPOSITION MODELING. Retrieved December 8, 2017, from https://sffsymposium.engr.utexas.edu/sites/default/files/2016/076-Hernandez.pdf

[15] Budynas, R. G., Nisbett, J. K., & Shigley, J. E. (2011). *Shigleys mechanical engineering design*. New York: McGraw-Hill.

VITA

Christian Trevino is from Del Rio, TX. She earned both a Bachelor's and Master's degree in Mechanical Engineering from The University of Texas at San Antonio.